Time-Varying Delayed Bilateral Teleoperation Without Force/Velocity Measurements

Time-Varying Delayed Bilateral Teleoperation Without Force/Velocity Measurements

Alejandro Gutierrez-Giles, Alejandro Rodriguez-Angeles, Philipp Schleer, and Marco A. Arteaga, *Member, IEEE*

***Abstract*— A bilateral teleoperation control scheme is proposed for the case of time-varying delays in the communication channel. The proposed scheme relies only on joint position measurements to estimate both velocities and external forces by using an extended-state high-gain observer. The estimated signals are in turn employed in a decentralized controller in a master–slave configuration. The control design is based on: 1) local force compensation, which improves the system stability; 2) direct force reflection, which increases the telepresence; and 3) only local damping injection, to deal with the instability problems arising from the time-varying delays in the communication while employing a simple three-channel architecture. A formal mathematical analysis is developed to guarantee the ultimate boundedness of estimation and tracking errors to an arbitrarily small region around zero. To test the validity of the proposed approach, experimental results are presented, including a comparison with an approach reported in the literature and a real-case communication over a long distance through the Internet.**

***Index Terms*— Disturbance observer (DOB), extended state, observer design, time-delayed teleoperation.**

I. Introduction

ROBOTIC teleoperation has been a very active area in the research community since the decade of 1960s with the seminal work of Goertz [1]. A major step was given in the late 1980s and the early 1990s with the works of Anderson and Spong [2] and Niemeyer and Slotine [3]. Several important results have been developed since then, as summarized in [4] up to 2022. The research efforts have been focused on different problems arising from robotic teleoperation. One of the most studied problems is varying time delays in the communication channel. In this context, several interesting results obtained by the passivity-based control technique were developed in the late 2000s, as summarized in [5]. The work presented in [6] improves these ideas by introducing several schemes that preserve passivity under both constant and variable time delays. Namnabat et al. [7] exploited the passivity assumption on the human and environment to propose a force-sensorless algorithm based on the generalized momentum estimator. The discrete-time case of passivity preservation for delayed systems is studied in [8]. Another interesting research direction is taken in [9], where a visual aid in the form of onomatopoeia is used for enhancing the performance of passivity-based teleoperation systems under time delays.

Concerning the problem of time delays in the communication channel, in [10], a robust controller, which cancels the dynamics of the manipulator by means of an adaptation law, is employed to enhance the transparency of the system. In [11], an impedance model reference adaptive controller is designed in a position-force teleoperation scheme. In [12], an extended-state observer (ESO) is used to estimate the lumped disturbances arising when achieving synchronization of the manipulators' positions. This is carried out by a sliding mode controller. However, a drawback of this work is that the controller relies on acceleration measurements. The same drawback is present in [13], where an adaptive controller with local force compensation at the slave side is proposed, and in [14], where a sliding mode controller with a disturbance observer (DOB) is utilized to achieve position-to-position tracking. In [15], a cascade linear observer is used to estimate and compensate time delays. In [16], a DOB is employed in a four-channel architecture to enhance the transparency of the system. In the same context, in [17], a scaled four-channel architecture in combination with a DOB is proposed to preserve the passivity of the closed-loop system. A simple algebraic criterium for stability is investigated by de Lima et al. [18], where they establish an algebraic formulation to determine the controller gains given the bounds on the delays and vice versa. In [19], an experimental study of a method that considers an explicit force control is presented for both nondelayed and delayed cases. A finite-time tracking controller for bilateral teleoperation without velocity measurements is proposed by Dao et al. [20], in which they consider nonpassive and bounded external forces. A neural network approach is proposed in [21] for the case of constant time delays, where frictions and external disturbances are estimated by an adaptive observer. Another work that proposes a neural

Manuscript received 29 November 2022; revised 28 August 2023; accepted 6 November 2023. Date of publication 1 December 2023; date of current version 25 April 2024. This work was supported in part by the Consejo Nacional de Humanidades Ciencias y Tecnologías (CONAHCYT) under Grant CB-2015-01/254329 and Grant CB2017-2018-A1-S-26123, in part by the Scholarship under Grant CVU:334785, and in part by the Dirección General de Asuntos del Personal Académico (DGAPA)-Universidad Nacional Autónoma de México (UNAM) under Project PAPIIT-IN102723. Recommended by Associate Editor A. Macchelli. *(Corresponding author: Alejandro Gutierrez-Giles.)*

Alejandro Gutierrez-Giles is with the Computer Sciences Department, Instituto Nacional de Astrofísica, Óptica y Electrónica (INAOE), Puebla 72840, Mexico (e-mail: alejandro.giles@inaoep.mx).

Alejandro Rodriguez-Angeles is with the Mechatronics Section, Centro de Investigación y Estudios Avanzados (Cinvestav), Mexico City 07360, Mexico, on sabbatical leave at the Mechanical Engineering Department, Dynamics and Control Group, Eindhoven University of Technology, 5612 AZ Eindhoven, The Netherlands (e-mail: aangeles@cinvestav.mx).

Philipp Schleer is with the Chair of Medical Engineering, Helmholtz Institute for Biomedical Engineering, RWTH Aachen University, 52074 Aachen, Germany (e-mail: schleer@hia.rwth-aachen.de).

Marco A. Arteaga is with the Electrical Engineering Division, Universidad Nacional Autónoma de México (UNAM), Mexico City 04510, Mexico (e-mail: marteagp@unam.mx).

Digital Object Identifier 10.1109/TCST.2023.3335748

network to estimate the upper bound of the time delay was presented recently in [22].

Force reflection is a very important feature that must be present in a teleoperation system because it is the fundamental contributor of telepresence, i.e., the sensation for the user to be manipulating the objects/environment at the remote side [23]. The works mentioned in the previous paragraph indirectly achieve a certain degree of force reflection, but this is not explicitly designed in the control law or guaranteed in the analysis. In this sense, in [24], a high-gain impedance adaptive controller is designed to reflect the contact force provided that a nonlinear model of the surface is available. In [25], a two-channel architecture (position force) is proposed to achieve enhanced transparency in an impedance controller scheme. In turn, in [26], the transparency in a four-channel architecture is investigated by using the passivity approach. A model predictive control approach is proposed in [27] for safe interaction with the environment while preserving transparency. Transparency for multilateral teleoperation with time delays is investigated by Tumerdem and Yilmaz [28], where they propose $\mathcal{L}_2$-stability-based criteria to achieve ideal transparency in such systems.

Another important research direction is the design of observers to estimate some of the involved variables such as velocity and force. There are many advantages obtained when replacing sensors by observers, e.g., weight and size reduction, costs, and maintenance. In this context, many works regarding the estimation of the robot velocities have been published. Though for position control of Lagrangian systems, observers are not strictly necessary, as stated in [29], there are still some advantages in estimating the internal states, such as velocities, e.g., for tuning. For example, in [30], an invariance and immersion (I&I) observer is employed in a position-to-position teleoperation scheme without explicit force reflection. Later, in [31], a linear velocity observer along with a proportional derivative (PD) controller is used to deal with the consensus problem of a network of robots. In a more recent paper [32], the same authors propose a nonlinear observer in conjunction with a nonlinear PD controller to provide robustness against disturbances and a good degree of transparency. In [33], a position-to-position robust adaptive controller is employed along with a linear observer to avoid velocity measurements.

On the other hand, force estimation has been a less addressed problem in the past but has gained focus in the last years. For example, in [34], a sliding mode observer and a sliding mode controller are proposed to simultaneously estimate the contact force and the velocities of both robots in an impedance-based teleoperation scheme. Later, in [35], an ESO is proposed based on a Kalman filter-like design over a linearized model. However, the conditions for stability required by the proposed controller and observer are difficult to check. Azimifar et al. [36], [37] proposed a force estimation algorithm plus a PD controller with local force compensation, which nevertheless relies on velocity and acceleration measurements. Next, in [38], a linear observer is designed to deal with the peaking phenomena, which is a well-known problem in high-gain observers applications. The estimated force is fed back to the operator in a linear controller scheme. In [39], a force estimation algorithm through a simple spring model is developed along with an admittance type controller for the case of no delays in the communication channel. In [40], a dynamic-gain extended-state force observer is employed in a four-channel architecture for the case of time-varying delays. In turn, in [41], a momentum observer is proposed to estimate both the environment and the operator forces. However, these two last schemes still need velocity measurements. A nonlinear observer is proposed in [42] to estimate external forces. In the same context, an adaptive observer in combination with a terminal sliding modes controller is proposed in [43]. Nevertheless, in both works, the estimated forces are not used for force reflection in the controller design.

In this work, we propose an observer-based three-channel teleoperation scheme. An extended-state high-gain observer is designed to simultaneously estimate the contact and the human operator forces, and the robot joint velocities. These signals are then employed in a three-channel position-force controller, with both local force compensation and force reflection. This is carried out by employing only joint position measurements. The ultimate boundedness of the estimated signals is guaranteed by a formal mathematical analysis.

The contributions of this work are listed as follows.

1) A force reflection is achieved by employing only position measurements while estimating velocities and forces.
2) Improved stability by local force compensation at the slave side and local damping injection at both sides.
3) The designed algorithm is easy to implement, it is computationally efficient, and it does not require a very fast sampling time.

The rest of this article is organized as follows. In Section II, a mathematical model of the teleoperation system along with some of its properties is presented, as well as some key assumptions. In Section III, the main result of this work is developed, i.e., the controller–observer design and mathematical analysis of the closed-loop dynamics. Then, in Section IV, some experimental results are presented to validate the proposed scheme, including a comparison study and a real scenario of intercontinental teleoperation through the Internet. Finally, in Section V, some concluding remarks and directions for future work are given.

Notation: Throughout the rest of this article, the subindex k means that the referred quantity is defined for both master and slave robots in the same way, i.e., $k = \{m, s\}$.

II. Mathematical Preliminaries

Consider the model of a master–slave teleoperation robotic system represented by the equations

$$\boldsymbol{H}_m(\boldsymbol{q}_{1\,m})\dot{\boldsymbol{q}}_{2\,m} + \boldsymbol{C}_m(\boldsymbol{q}_{1\,m}, \boldsymbol{q}_{2\,m})\boldsymbol{q}_{2\,m} + \boldsymbol{g}_m(\boldsymbol{q}_{1\,m}) = \boldsymbol{\tau}_m + \boldsymbol{\tau}_h \tag{1}$$

$$\boldsymbol{H}_s(\boldsymbol{q}_{1\,s})\dot{\boldsymbol{q}}_{2\,s} + \boldsymbol{C}_s(\boldsymbol{q}_{1\,s}, \boldsymbol{q}_{2\,s})\boldsymbol{q}_{2\,s} + \boldsymbol{g}_s(\boldsymbol{q}_{1\,s}) = \boldsymbol{\tau}_s - \boldsymbol{\tau}_e \tag{2}$$

where, for $k = m$ and s, $\boldsymbol{q}_{1k} \triangleq \boldsymbol{q}_k$ stand for the manipulators joint positions, $\boldsymbol{q}_{2k} \triangleq \dot{\boldsymbol{q}}_k$ are the joint velocities, $\boldsymbol{H}_k(\boldsymbol{q}_{1\,k}) \in \mathbb{R}^{n\times n}$ is the inertia matrix, $\boldsymbol{C}_k(\boldsymbol{q}_{1\,k}, \boldsymbol{q}_{2\,k})\boldsymbol{q}_{2\,k} \in \mathbb{R}^n$ is the vector of Coriolis and centrifugal torques, $\boldsymbol{g}_k(\boldsymbol{q}_{1\,k}) \in \mathbb{R}^n$ is

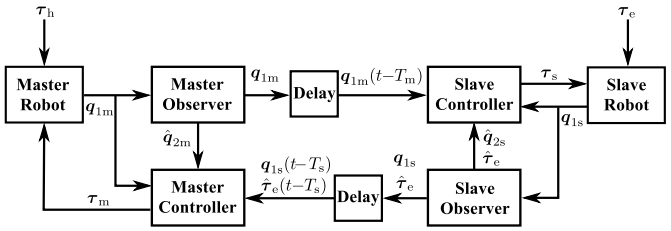

Fig. 1. Block diagram of the observer-based three-channel teleoperation scheme.

the gravity torque, and $\boldsymbol{\tau}_m, \boldsymbol{\tau}_s \in \mathbb{R}^n$ are the control inputs. The torque imposed by the human operator over the master robot is $\boldsymbol{\tau}_h \in \mathbb{R}^n$, while the external torque exerted by the slave robot over a remote environment[1] is written as $\boldsymbol{\tau}_e \in \mathbb{R}^n$. This model satisfies the following standard properties [45, Sec. 3.4].

Property 1: The inertia matrices $\boldsymbol{H}_k(\boldsymbol{q}_{1k})$ are symmetric and positive definite and satisfy $\lambda_h(\boldsymbol{q}_{1k})\|\boldsymbol{x}\|^2 \leq \boldsymbol{x}^T\boldsymbol{H}_k(\boldsymbol{q}_{1k})\boldsymbol{x} \leq \lambda_H(\boldsymbol{q}_{1k})\|\boldsymbol{x}\|^2$, for all $\boldsymbol{x} \in \mathbb{R}^n$ and scalar functions $0 < \lambda_h(\boldsymbol{q}_{1k}) \leq \lambda_H(\boldsymbol{q}_{1k}) < \infty$. Moreover, if the manipulators have only revolute joints, these functions are independent of the configuration, i.e., $\lambda_h\|\boldsymbol{x}\|^2 \leq \boldsymbol{x}^T\boldsymbol{H}_k(\boldsymbol{q}_{1k})\boldsymbol{x} \leq \lambda_H\|\boldsymbol{x}\|^2$ for $0 < \lambda_h \leq \lambda_H < \infty$. □

Property 2: By employing the Christoffel symbols of the first kind to compute $\boldsymbol{C}_k(\boldsymbol{q}_{1k}, \boldsymbol{q}_{2k})$, the matrix $\dot{\boldsymbol{H}}_k(\boldsymbol{q}_{1k}) - 2\boldsymbol{C}_k(\boldsymbol{q}_{1k}, \boldsymbol{q}_{2k})$ is skew-symmetric. □

Property 3: For $\boldsymbol{q}, \boldsymbol{x}, \boldsymbol{y} \in \mathbb{R}^n$, the vector $\boldsymbol{C}_k(\boldsymbol{q}, \boldsymbol{x})\boldsymbol{y}$ satisfies

$$\boldsymbol{C}_k(\boldsymbol{q}, \boldsymbol{x})\boldsymbol{y} = \boldsymbol{C}_k(\boldsymbol{q}, \boldsymbol{y})\boldsymbol{x}. \tag{3}$$

□

The following assumption is made to simplify the analysis of Section III.

Assumption 1: The master and slave manipulators have only revolute joints. □

To design the subsequent controllers and state estimators, we write down the dynamics (1) and (2) in a state-space form as

$$\dot{\boldsymbol{q}}_{1k} = \boldsymbol{q}_{2k} \tag{4}$$

$$\dot{\boldsymbol{q}}_{2k} = \boldsymbol{H}_k^{-1}(\boldsymbol{q}_{1k})\big(\boldsymbol{\tau}_k - \boldsymbol{C}_k(\boldsymbol{q}_{1k}, \boldsymbol{q}_{2k})\boldsymbol{q}_{2k} - \boldsymbol{g}(\boldsymbol{q}_{1k})\big) + \boldsymbol{z}_{1k} \tag{5}$$

where $\boldsymbol{z}_{1k} \in \mathbb{R}^n$ represents the external forces terms defined by

$$\boldsymbol{z}_{1\,m} \triangleq \boldsymbol{H}_m^{-1}(\boldsymbol{q}_{1\,m})\boldsymbol{\tau}_h \tag{6}$$

$$\boldsymbol{z}_{1\,s} \triangleq -\boldsymbol{H}_s^{-1}(\boldsymbol{q}_{1\,s})\boldsymbol{\tau}_e. \tag{7}$$

To estimate the external forces and joint velocities, the following assumptions are made.

Assumption 2: Each vector $\boldsymbol{z}_{1k}$ can be expressed as a time polynomial of degree $p-1$ plus a residual term, i.e.,

$$\boldsymbol{z}_{1k} = \sum_{i=1}^{p-1} \boldsymbol{a}_{ik} t^i + \boldsymbol{r}_k(t) \tag{8}$$

[1]For the sake of simplicity, it is considered that the external forces are directly the torques at the robot joints, which implies that the manipulators must be kinematically similar. This assumption can be easily removed by working directly in Cartesian coordinates and by mapping the external forces via the well-known relationship $\boldsymbol{\tau}_e = \boldsymbol{J}^T(\boldsymbol{q}_{1\,s})\boldsymbol{F}_e$ [44, Sec. 3.8].

where each $\boldsymbol{a}_{ik} \in \mathbb{R}^n$ is a vector of constant coefficients and $\boldsymbol{r}_k(t) \in \mathbb{R}^n$ is the residual vector. □

Assumption 3: At least the first p time derivatives ($p \geq 1$) of $\boldsymbol{z}_{1m}$ and $\boldsymbol{z}_{1s}$ are bounded. □

After the last two assumptions, the internal model for the extended state can be written as

$$\dot{\boldsymbol{z}}_{1k} = \boldsymbol{z}_{2k} \tag{9}$$

$$\dot{\boldsymbol{z}}_{2k} = \boldsymbol{z}_{3k} \tag{10}$$

$$\vdots$$

$$\dot{\boldsymbol{z}}_{\mathrm{pk}} = \boldsymbol{r}_k^{(p)}(t). \tag{11}$$

When there are delays in the communication channel, the necessary signals to synchronize the trajectories of the robots as well as to provide an accurate sensation of the remote environment to the human operator through force feedback are not instantly available, but only after the time delay, as shown in Fig. 1. Thus, the master position and velocity signals, which are the references for the slave manipulator are delayed by a time T_m, whereas the signals that are transmitted back to the master manipulator side are delayed by a time T_s. In this work, the control objective is twofold: position tracking and force feedback. In the first case, it is intended for the slave robot to follow the master movements, though after the delay imposed by the communication channel, i.e., the position control objective is to drive $\boldsymbol{q}_s - \boldsymbol{q}_m$ as close to zero as possible in steady state. On the other hand, the force feedback objective can be translated for the human operator to feel the force exerted by the slave robot over the remote environment, though transmitted by the manipulators' torque, i.e., to drive $\boldsymbol{\tau}_h - \boldsymbol{\tau}_e(t - T_s(t))$ close to zero also in steady state.

Remark 1: While transparency is an established concept for nondelayed teleoperation through impedance matching or kinematic correspondence, for time-varying delayed teleoperation, there is not a universally accepted criterium to establish transparency. Following the definitions of [46], which are further investigated in [32] for time-delayed systems, there can be defined three ideal responses: 1) a kinematic unilateral delayed correspondence, i.e., $\boldsymbol{q}_s \to \boldsymbol{q}_m(t - T_m(t))$; 2) a unilateral force delayed correspondence, i.e., $\boldsymbol{\tau}_m \to \boldsymbol{\tau}_s(t - T_m(t))$; and 3) a combination of 1) and 2). Although ideal case 3) is the best option, it is difficult to establish for the proposed scheme since we are not transmitting velocities through the communication channel. Thus, in this work, we aim at obtaining the force delayed correspondence 2) in steady state. □

The following assumption is made concerning the time-varying delays in the communication channel.

Assumption 4: The time-varying delays $T_m(t)$ and $T_s(t)$ are bounded, i.e., $\max_{t \geq t_0} T_m(t) \leq c_{\mathrm{Tm}}$ and $\max_{t \geq t_0} T_s(t) \leq c_{\mathrm{Ts}}$, for some known constants $c_{\mathrm{Tm}}, c_{\mathrm{Ts}} \geq 0$.

III. Controller and Observer Design

The main contribution of this work is the use of estimated signals instead of measured ones. There are several advantages to doing so, such as diminution of weight/volume, cost reduction, and less additional equipment. Specifically, the contact force and the joint velocities required for the teleoperation

algorithm are estimated based on joint position measurements and input torques. To estimate these signals, we employ the extended-state high-gain observer taken from [47]

$$\dot{\hat{\boldsymbol{q}}}_{1k} = \hat{\boldsymbol{q}}_{2k} + \lambda_{p+1}\tilde{\boldsymbol{q}}_{1k} \tag{12}$$

$$\dot{\hat{\boldsymbol{q}}}_{2k} = \boldsymbol{H}_k^{-1}(\boldsymbol{q}_{1k})\big(\boldsymbol{\tau}_k - \boldsymbol{C}_k(\boldsymbol{q}_{1k}, \hat{\boldsymbol{q}}_{2k})\hat{\boldsymbol{q}}_{2k} - \boldsymbol{g}(\boldsymbol{q}_{1k})\big) + \hat{\boldsymbol{z}}_{1k} + \lambda_p\tilde{\boldsymbol{q}}_{1k} \tag{13}$$

$$\dot{\hat{\boldsymbol{z}}}_{1k} = \hat{\boldsymbol{z}}_{2k} + \lambda_{p-1}\tilde{\boldsymbol{q}}_{1k} \tag{14}$$

$$\dot{\hat{\boldsymbol{z}}}_{2k} = \hat{\boldsymbol{z}}_{3k} + \lambda_{p-2}\tilde{\boldsymbol{q}}_{1k} \tag{15}$$

$$\vdots$$

$$\dot{\hat{\boldsymbol{z}}}_{\mathrm{pk}} = \lambda_0\tilde{\boldsymbol{q}}_{1k} \tag{16}$$

where $\tilde{\boldsymbol{q}}_{1k} \triangleq \boldsymbol{q}_{1k} - \hat{\boldsymbol{q}}_{1k}$ is the observation error and

$$\tilde{\boldsymbol{q}}_{2k} \triangleq \boldsymbol{q}_{2k} - \hat{\boldsymbol{q}}_{2k} \tag{17}$$

$$\tilde{\boldsymbol{z}}_{jk} \triangleq \boldsymbol{z}_{jk} - \hat{\boldsymbol{z}}_{jk}, \quad j = 1, \ldots, p. \tag{18}$$

Moreover, the phase state of the observation error can be grouped into the vector

$$\boldsymbol{x}_{\mathrm{ok}} \triangleq \begin{bmatrix} \tilde{\boldsymbol{q}}_{1k} & \dot{\tilde{\boldsymbol{q}}}_{1k} & \cdots & \tilde{\boldsymbol{q}}_{1k}^{(p+1)} \end{bmatrix}^T. \tag{19}$$

From these observers, it is possible to obtain an estimate of the joint velocities $\hat{\boldsymbol{q}}_{2k}$. The estimation of the external forces can be obtained as well since, from (6) to (7), it is

$$\hat{\boldsymbol{\tau}}_h = \boldsymbol{H}_m(\boldsymbol{q}_{1\,m})\hat{\boldsymbol{z}}_{1\,m} \tag{20}$$

$$\hat{\boldsymbol{\tau}}_e = -\boldsymbol{H}_s(\boldsymbol{q}_{1\,s})\hat{\boldsymbol{z}}_{1\,s}. \tag{21}$$

Therefore, the observer-based control laws for both master and slave manipulators proposed in this work are

$$\boldsymbol{\tau}_m = -\boldsymbol{K}_{\mathrm{vm}}\hat{\boldsymbol{q}}_{2\,m} - \boldsymbol{K}_{\mathrm{pm}}\big(\boldsymbol{q}_{1\,m} - \boldsymbol{q}_{1\,s}(t - T_s(t))\big) - \hat{\boldsymbol{\tau}}_e(t - T_s(t)) + \boldsymbol{g}_m(\boldsymbol{q}_{1\,m}) \tag{22}$$

$$\boldsymbol{\tau}_s = -\boldsymbol{K}_{\mathrm{vs}}\hat{\boldsymbol{q}}_{2\,s} - \boldsymbol{K}_{\mathrm{ps}}\big(\boldsymbol{q}_{1\,s} - \boldsymbol{q}_{1\,m}(t - T_m(t))\big) + \hat{\boldsymbol{\tau}}_e + \boldsymbol{g}_s(\boldsymbol{q}_{1\,s}) \tag{23}$$

where $\boldsymbol{K}_{\mathrm{vm}}, \boldsymbol{K}_{\mathrm{pm}}, \boldsymbol{K}_{\mathrm{vs}}, \boldsymbol{K}_{\mathrm{vm}} \in \mathbb{R}^{n\times n}$ are positive definite matrices of constant gains.

A. Stability Analysis

By combining the state-space model (4) and (5), the internal model (9)–(11), and the proposed observer (12)–(16), one can obtain the observation error dynamics

$$\dot{\tilde{\boldsymbol{q}}}_{1k} = \tilde{\boldsymbol{q}}_{2k} - \lambda_{p+1}\tilde{\boldsymbol{q}}_{1k} \tag{24}$$

$$\dot{\tilde{\boldsymbol{q}}}_{2k} = \boldsymbol{f}_{c_k} + \tilde{\boldsymbol{z}}_{1k} - \lambda_p\tilde{\boldsymbol{q}}_{1k} \tag{25}$$

$$\dot{\tilde{\boldsymbol{z}}}_{1k} = \tilde{\boldsymbol{z}}_{2k} - \lambda_{p-1}\tilde{\boldsymbol{q}}_{1k} \tag{26}$$

$$\vdots$$

$$\dot{\tilde{\boldsymbol{z}}}_{\mathrm{pk}} = \boldsymbol{r}_k^{(p)}(t) - \lambda_0\tilde{\boldsymbol{q}}_{1k} \tag{27}$$

with

$$\begin{aligned}\boldsymbol{f}_{c_k} &\triangleq \boldsymbol{H}_k^{-1}(\boldsymbol{q}_{1k})\big(\boldsymbol{C}_k(\boldsymbol{q}_{1k}, \hat{\boldsymbol{q}}_{2k})\hat{\boldsymbol{q}}_{2k} - \boldsymbol{C}_k(\boldsymbol{q}_{1k}, \boldsymbol{q}_{2k})\boldsymbol{q}_{2k}\big)\\ &= \boldsymbol{H}_k^{-1}(\boldsymbol{q}_{1k})\big(\boldsymbol{C}_k(\boldsymbol{q}_{1k}, \tilde{\boldsymbol{q}}_{2k})\tilde{\boldsymbol{q}}_{2k} - 2\boldsymbol{C}_k(\boldsymbol{q}_{1k}, \boldsymbol{q}_{2k})\tilde{\boldsymbol{q}}_{2k}\big)\end{aligned} \tag{28}$$

where the last equality is obtained by repeatedly applying Property 3. On the other hand, the closed-loop dynamics of model (4) and (5) under the action of the control laws (22) and (23) is

$$\begin{aligned}\dot{\boldsymbol{q}}_{2\,m} = \boldsymbol{H}_m^{-1}(\boldsymbol{q}_{1\,m})\big[&-\boldsymbol{C}_m(\boldsymbol{q}_{1\,m}, \boldsymbol{q}_{2\,m})\boldsymbol{q}_{2\,m} - \boldsymbol{K}_{\mathrm{vm}}\hat{\boldsymbol{q}}_{2m}\\ &- \boldsymbol{K}_{\mathrm{pm}}\big(\boldsymbol{q}_{1\,m} - \boldsymbol{q}_{1\,s}(t - T_s(t))\big)\\ &+ \boldsymbol{\tau}_h - \hat{\boldsymbol{\tau}}_e(t - T_s(t))\big]\end{aligned} \tag{29}$$

$$\begin{aligned}\dot{\boldsymbol{q}}_{2\,s} = \boldsymbol{H}_s^{-1}(\boldsymbol{q}_{1\,s})\big[&-\boldsymbol{C}_s(\boldsymbol{q}_{1\,s}, \boldsymbol{q}_{2\,s})\boldsymbol{q}_{2\,s} - \boldsymbol{K}_{\mathrm{vs}}\hat{\boldsymbol{q}}_{2\,s}\\ &- \boldsymbol{K}_{\mathrm{ps}}\big(\boldsymbol{q}_{1\,s} - \boldsymbol{q}_{1\,m}(t - T_m(t))\big) + \tilde{\boldsymbol{\tau}}_e\big]\end{aligned} \tag{30}$$

where $\tilde{\boldsymbol{\tau}}_e \triangleq \boldsymbol{\tau}_e - \hat{\boldsymbol{\tau}}_e$.

For the subsequent development, let us lump together the states that define both the observation errors and the motion dynamics into a vector $\boldsymbol{x} \in \mathbb{R}^{3n+2(p+2)}$ as

$$\boldsymbol{x} \triangleq \begin{bmatrix} \boldsymbol{e} & \boldsymbol{q}_{2\,m} & \boldsymbol{q}_{2\,s} & \boldsymbol{x}_{\mathrm{om}} & \boldsymbol{x}_{\mathrm{os}} \end{bmatrix}^T \tag{31}$$

where $\boldsymbol{e} = \boldsymbol{q}_{1\,m} - \boldsymbol{q}_{1\,s}$. The next assumption is made regarding the state initial condition for time-delayed systems.

Assumption 5: The initial state prior to the maximum bound on the master and slave time delays is zero, i.e.,

$$\boldsymbol{x}(t_0 + \sigma) = \boldsymbol{0} \quad \forall\sigma \in [-c_{\mathrm{TM}}, 0] \tag{32}$$

where $c_{\mathrm{TM}} = \max\{c_{\mathrm{Tm}}, c_{\mathrm{Ts}}\}$. □

Although this assumption is made to simplify the analysis, it is not restrictive from the practical point of view since the robots can be initialized in a known position and wait for a time $t \geq c_{\mathrm{TM}}$ before starting the task.

The next lemma states that boundedness on this vector implies boundedness of all signals of interest.

Lemma 1: Consider the region $\mathcal{B}_r \triangleq \{\boldsymbol{x} \in \mathbb{R}^{3n+2(p+2)} : \|\boldsymbol{x}\| \leq x_{\max}\}$ and suppose that Assumptions 1–3 are satisfied. If $\boldsymbol{x}(t) \in \mathcal{B}_r$, then every signal of interest (i.e., $\boldsymbol{q}_{2k}, \dot{\boldsymbol{q}}_{2k}, \ldots, \boldsymbol{q}_{2k}^{(p)}$, $\hat{\boldsymbol{q}}_{2k}, \dot{\hat{\boldsymbol{q}}}_{2k}, \ldots, \hat{\boldsymbol{q}}_{2k}^{(p)}$, $\boldsymbol{f}_{c_k}, \dot{\boldsymbol{f}}_{c_k}, \ldots, \boldsymbol{f}_{c_k}^{(p)}$, $\tilde{\boldsymbol{z}}_{1\,k}, \dot{\tilde{\boldsymbol{z}}}_{1\,k}, \ldots, \tilde{\boldsymbol{z}}_{1\,k}^{(p)}$, $\hat{\boldsymbol{z}}_{1\,k}, \dot{\hat{\boldsymbol{z}}}_{1\,k}, \ldots, \hat{\boldsymbol{z}}_{1\,k}^{(p)}$, $\hat{\boldsymbol{\tau}}_h, \dot{\hat{\boldsymbol{\tau}}}_h, \ldots, \hat{\boldsymbol{\tau}}_h^{(p)}$, and $\hat{\boldsymbol{\tau}}_e, \dot{\hat{\boldsymbol{\tau}}}_e, \ldots, \hat{\boldsymbol{\tau}}_e^{(p)}$, for $k = m, s$) is bounded.

Proof: From (24), one has directly $\tilde{\boldsymbol{q}}_{2\,m}, \tilde{\boldsymbol{q}}_{2\,s} \in \mathcal{L}_\infty$. In fact, for $k = m, s$, by taking the first p time derivatives of (24), one obtains $\dot{\tilde{\boldsymbol{q}}}_{2k}, \ddot{\tilde{\boldsymbol{q}}}_{2k}, \ldots, \tilde{\boldsymbol{q}}_{2k}^{(p)} \in \mathcal{L}_\infty$. After the observation error definition (17), $\hat{\boldsymbol{q}}_{2k} \in \mathcal{L}_\infty$. Now, since $\boldsymbol{f}_{c_k} = \boldsymbol{f}_{c_k}(\boldsymbol{q}_{1k}, \boldsymbol{q}_{2\,k}, \tilde{\boldsymbol{q}}_{2k})$ in (28) is a continuous function in $\mathcal{B}_r$, it must be[2] $\boldsymbol{f}_{c_k} \in \mathcal{L}_\infty$, and thus, it must be $\tilde{\boldsymbol{z}}_{1k}$ in (25). From definition (18) and Assumption 3, $\hat{\boldsymbol{z}}_{1k} \in \mathcal{L}_\infty$ and so are $\hat{\boldsymbol{\tau}}_h, \hat{\boldsymbol{\tau}}_e$ in (20) and (21). Since, for $j = 1, 2$ [49, p. 80]

$$\boldsymbol{q}_{1k}\big(t - T_j(t)\big) = \boldsymbol{q}_{1k}(t) - \int_{t-T_j(t)}^{t} \boldsymbol{q}_{2k}(\sigma)d\sigma \tag{33}$$

the closed-loop equations (29) and (30) can be rewritten as[3]

$$\begin{aligned}\dot{\boldsymbol{q}}_{2\,m} = \boldsymbol{H}_m^{-1}(\boldsymbol{q}_{1\,m})\Big(&-\boldsymbol{C}_m(\boldsymbol{q}_{1\,m}, \boldsymbol{q}_{2\,m})\boldsymbol{q}_{2\,m} - \boldsymbol{K}_{\mathrm{vm}}\boldsymbol{q}_{2m}\\ &- \boldsymbol{K}_{\mathrm{pm}}\boldsymbol{e} + \boldsymbol{K}_{\mathrm{vm}}\tilde{\boldsymbol{q}}_{2\,m} + \boldsymbol{\tau}_h - \hat{\boldsymbol{\tau}}_e(t - T_s)\end{aligned}$$

[2]Note that even if $\boldsymbol{q}_{1k}$ is not bounded, the function $\boldsymbol{f}_{c_k}$ remains bounded since $\boldsymbol{q}_{1k}$ enters the matrix $\boldsymbol{C}_k(\boldsymbol{q}_{1k}, \boldsymbol{y})$ through sinusoidal functions for manipulators with only revolute joints [48].

[3]For simplicity's sake, from now on we write T_m and T_s instead of $T_m(t)$ and $T_s(t)$.

$$+\boldsymbol{K}_{\text{pm}}\int_{t-T_s}^{t}\boldsymbol{q}_{2\,s}(\sigma)d\sigma\Big) \tag{34}$$

$$\dot{\boldsymbol{q}}_{2\,s}=\boldsymbol{H}_s^{-1}(\boldsymbol{q}_{1\,s})\Big(-\boldsymbol{C}_s(\boldsymbol{q}_{1\,s},\boldsymbol{q}_{2\,s})\boldsymbol{q}_{2\,s}-\boldsymbol{K}_{\text{vs}}\boldsymbol{q}_{2s}+\boldsymbol{K}_{\text{ps}}\boldsymbol{e}$$
$$+\boldsymbol{K}_{\text{vs}}\tilde{\boldsymbol{q}}_{2\,s}+\tilde{\boldsymbol{\tau}}_e+\boldsymbol{K}_{\text{ps}}\int_{t-T_m}^{t}\boldsymbol{q}_{2\,m}(\sigma)d\sigma\Big). \tag{35}$$

Since $\boldsymbol{q}_{2\,m}$ and $\boldsymbol{q}_{2\,s}$ are bounded in $\mathcal{B}_r$, by the mean value theorem, $\int_{t-T_m}^{t}\boldsymbol{q}_{2\,m}(\sigma)d\sigma \le x_{\max}c_{\text{Tm}}$ and $\int_{t-T_s}^{t}\boldsymbol{q}_{2\,s}(\sigma)d\sigma \le x_{\max}c_{\text{Ts}}$. As a consequence, $\dot{\boldsymbol{q}}_{2\,s}\in\mathcal{L}_\infty$, which in turn implies that $\dot{\hat{\boldsymbol{q}}}_{2\,s}\in\mathcal{L}_\infty$, as $\dot{\tilde{\boldsymbol{q}}}_{2\,s}\in\mathcal{L}_\infty$. By taking the time derivative of (25) and (28) for $k=s$, it follows $\dot{\tilde{z}}_{1s}\in\mathcal{L}_\infty$ and, after Assumption 3, it is $\dot{\hat{z}}_{1s}$. Therefore, $\dot{\boldsymbol{q}}_{2\,m}\in\mathcal{L}_\infty$ in (34).

From this point, an iterative procedure can be followed. By denoting by $(\cdot)^{(i)}$ the ith time derivative, it follows that $\boldsymbol{q}_{2\,m}^{(i)},\boldsymbol{q}_{2\,s}^{(i)}\in\mathcal{L}_\infty$ implies $\hat{\boldsymbol{q}}_{2\,m}^{(i)},\hat{\boldsymbol{q}}_{2\,s}^{(i)}\in\mathcal{L}_\infty$ through (17), and also, $\boldsymbol{f}_{c_k}^{(i)}\in\mathcal{L}_\infty$, since the ith time derivative of $\boldsymbol{f}_{c_k}=\boldsymbol{f}_{c_k}(\boldsymbol{q}_{1k},\boldsymbol{q}_{2\,k},\ldots,\boldsymbol{q}_{2\,k}^{(i)},\tilde{\boldsymbol{q}}_{2k},\ldots,\tilde{\boldsymbol{q}}_{2k}^{(i)})$ in (28). Next, by taking the ith time derivative of (25), it implies that $\tilde{z}_{1k}^{(i)}\in\mathcal{L}_\infty$. Now, by considering Assumption 3 and the ith time derivative of (18), (20), and (21), $\tilde{z}_{1k}^{(i)}\in\mathcal{L}_\infty$ implies that $\hat{z}_{1k}^{(i)},\hat{\boldsymbol{\tau}}_h^{(i)},\hat{\boldsymbol{\tau}}_e^{(i)}\in\mathcal{L}_\infty$. This also implies, after (34) and (35), that $\boldsymbol{q}_{2k}^{(i+1)}\in\mathcal{L}_\infty$, and the iteration starts again. The iteration stops at $i=p$. Therefore, $\boldsymbol{q}_{2k},\dot{\boldsymbol{q}}_{2k},\ldots,\boldsymbol{q}_{2k}^{(p)},\hat{\boldsymbol{q}}_{2k},\dot{\hat{\boldsymbol{q}}}_{2k},\ldots,\hat{\boldsymbol{q}}_{2k}^{(p)},\boldsymbol{f}_{c_k},\dot{\boldsymbol{f}}_{c_k},\ldots,\boldsymbol{f}_{c_k}^{(p)},\tilde{\boldsymbol{z}}_{1\,k},\dot{\tilde{\boldsymbol{z}}}_{1\,k},\ldots,\tilde{\boldsymbol{z}}_{1\,k}^{(p)},\hat{\boldsymbol{z}}_{1\,k},\dot{\hat{\boldsymbol{z}}}_{1\,k},\ldots,\hat{\boldsymbol{z}}_{1\,k}^{(p)},\hat{\boldsymbol{\tau}}_h,\dot{\hat{\boldsymbol{\tau}}}_h,\ldots,\hat{\boldsymbol{\tau}}_h^{(p)}$, and $\hat{\boldsymbol{\tau}}_e,\dot{\hat{\boldsymbol{\tau}}}_e,\ldots,\hat{\boldsymbol{\tau}}_e^{(p)}$ are bounded. ■

Remark 2: Care should be taken when using Lemma 1. It barely claims that, should the state $\boldsymbol{x}(t)$ be bounded, then any other signal or variable of interest must be bounded as well. This, however, does not mean that the state $\boldsymbol{x}(t)$ is assumed to be bounded. Its boundedness has to be proven and even enforced by gain choosing. As it will be shown later, Lemma 1 helps to achieve this goal because it allows showing that finite control/observer gains can always be found to keep $\boldsymbol{x}(t)\in\mathcal{B}_r,\forall t\ge t_0$ for some $\boldsymbol{x}(t_0)\in\mathcal{S}\subseteq\mathcal{B}_r$ (but not necessarily for *all* $\boldsymbol{x}(t_0)\in\mathcal{B}_r$). This, of course, means that the stability analysis is only local and valid for the region of interest $\mathcal{B}_r$. Finally, note that Assumption 3 could be dropped by the more relaxed assumption that the first p derivatives of z_{1m} and z_{1s} exist, but this is at the cost of making the proof of Lemma 1 by far more complex. See [50] for details. □

By combining the equations of the observation error dynamics (24)–(27), it is straightforward to obtain the differential equation

$$\tilde{\boldsymbol{q}}_{1k}^{(p+2)}+\lambda_{p+1}\tilde{\boldsymbol{q}}_{1k}^{(p+1)}+\cdots+\lambda_0\tilde{\boldsymbol{q}}_{1k}=\boldsymbol{r}_k^{(p)}(t)+\boldsymbol{f}_{c_k}^{(p)} \tag{36}$$

which shows that $\tilde{\boldsymbol{q}}_{1k}^{(p+2)}\in\mathcal{L}_\infty$. Moreover, from the theory of linear systems under bounded inputs, (36) shows that $\tilde{\boldsymbol{q}}_{1k}$ and its first $p+2$ time derivatives can be made arbitrarily small by choosing the diagonal gain matrices λ_i such that the vector polynomial

$$s^{(p+2)}+\lambda_{p+1}s^{(p+1)}+\cdots+\lambda_0 s=\boldsymbol{0} \tag{37}$$

is Hurwitz with roots located as far as possible on the left half of the complex plane [51, p. 21]. Furthermore, this also means that $\tilde{\boldsymbol{q}}_{2k}$ and its first p time derivatives can be made arbitrarily small as well, which in turn implies that $\boldsymbol{f}_{c_k},\dot{\boldsymbol{f}}_{c_k},\ldots,\boldsymbol{f}_{c_k}^{(p)}$ can also be made arbitrarily small, regardless of any other parameters or gains different than the observer gains in (12)–(16).

By considering the vector definition of the observation error phase state (19), the dynamics (36) for $k=m$ and s can be written as

$$\dot{\boldsymbol{x}}_{\text{ok}}=\boldsymbol{A}_{\text{ok}}\boldsymbol{x}_{\text{ok}}+\boldsymbol{B}_{\text{ok}}\boldsymbol{u}_{\text{rfk}} \tag{38}$$

with

$$\boldsymbol{A}_{\text{ok}}=\begin{bmatrix}\boldsymbol{O}&\boldsymbol{I}&\boldsymbol{O}&\cdots&\boldsymbol{O}\\ \boldsymbol{O}&\boldsymbol{O}&\boldsymbol{I}&\cdots&\boldsymbol{O}\\ &\vdots&&\ddots&\vdots\\ \boldsymbol{O}&\boldsymbol{O}&\boldsymbol{O}&\cdots&\boldsymbol{I}\\ -\lambda_0&-\lambda_1&-\lambda_2&\cdots&-\lambda_{p+1}\end{bmatrix} \tag{39}$$

$$\boldsymbol{B}_{\text{ok}}=\begin{bmatrix}\boldsymbol{O}&\boldsymbol{O}&\cdots&\boldsymbol{O}&\boldsymbol{I}\end{bmatrix}^T \tag{40}$$

$$\boldsymbol{u}_{\text{rfk}}=\boldsymbol{r}_k^{(p)}(t)+\boldsymbol{f}_{c_k}^{(p)}. \tag{41}$$

As mentioned in Remark 2, the stability analysis is intended to be only local and valid for the region $\mathcal{B}_r$. Therefore, for that case there exists a scalar c_{b1} such that $\|\boldsymbol{u}_{\text{rfk}}\|\le c_{b1}$ in $\mathcal{B}_r$. Once again, care should be taken because the bound c_{b1} loses its validity in case $\boldsymbol{x}$ leaves $\mathcal{B}_r$, but as it will be shown later, a region of attraction can always be found so that this never happens. On the other hand, it is well known from a basic result of linear systems [52, p. 136] that since the unforced part of (38) is asymptotically stable, it satisfies the Lyapunov equation

$$\boldsymbol{A}_{\text{ok}}^T\boldsymbol{P}_{\text{ok}}+\boldsymbol{P}_{\text{ok}}\boldsymbol{A}_{\text{ok}}=-\boldsymbol{Q}_{\text{ok}} \tag{42}$$

where $\boldsymbol{P}_{\text{ok}},\boldsymbol{Q}_{\text{ok}}\in\mathbb{R}^{(p+2)\times(p+2)}$ are symmetric positive definite matrices. Now, consider the positive definite functions

$$V_{\text{ok}}=\boldsymbol{x}_{\text{ok}}^T\boldsymbol{P}_{\text{ok}}\boldsymbol{x}_{\text{ok}}. \tag{43}$$

The derivative of these functions along the trajectories of (38) is given by

$$\dot{V}_{\text{ok}}=-\boldsymbol{x}_{\text{ok}}^T\boldsymbol{Q}_{\text{ok}}\boldsymbol{x}_{\text{ok}}+2\boldsymbol{x}_{\text{ok}}^T\boldsymbol{P}_{\text{ok}}\boldsymbol{B}_{\text{ok}}\boldsymbol{u}_{\text{rfk}}$$
$$\le-\|\boldsymbol{x}_{\text{ok}}\|\big(\lambda_{\min}\big(\boldsymbol{Q}_{\text{ok}}\big)\|\boldsymbol{x}_{\text{ok}}\|-2\lambda_{\max}(\boldsymbol{P}_{\text{ok}})\|\boldsymbol{B}_{\text{ok}}\|c_{b1}\big) \tag{44}$$

where $\lambda_{\min}(\cdot)$ and $\lambda_{\max}(\cdot)$ represent the minimum and the maximum eigenvalue of their arguments, respectively. Therefore,

$$\dot{V}_{\text{ok}}\le 0,\quad \text{if } \|\boldsymbol{x}_{\text{ok}}\|\ge 2\frac{\lambda_{\max}(\boldsymbol{P}_{\text{ok}})}{\lambda_{\min}\big(\boldsymbol{Q}_{\text{ok}}\big)}\|\boldsymbol{B}_{\text{ok}}\|c_{b1}. \tag{45}$$

Remark 3: As shown in [47], the factor $\lambda_{\max}(\boldsymbol{P}_{\text{ok}})/\lambda_{\min}(\boldsymbol{Q}_{\text{ok}})$ can be made arbitrarily small with proper tuning of the observer gains in (12)–(16). This in turn implies that the observation errors can be made arbitrarily small, which prevents leaving $\mathcal{B}_r$. □

Now, we state the main result of this work.

Proposition 1: Consider the master–slave teleoperation system described by (1) and (2) in closed loop with the observers (12)–(16), for both master and slave robots, and the control laws (22) and (23). Assume that the manipulators satisfy Assumption 1 and the external forces $\boldsymbol{\tau}_h$ and $\boldsymbol{\tau}_e$ satisfy Assumptions 2 and 3. Then, there exists a constant $d_r>0$ such

that if $\|\boldsymbol{x}(t_0)\| < d_r$, the following conditions hold: 1) a combination of controllers and observers gains can always be found such that the state (31) is ultimately bounded and 2) the manipulators' velocities $\dot{\boldsymbol{q}}_m$ and $\dot{\boldsymbol{q}}_s$ can be ultimately bounded by an arbitrarily small disk around zero.

Proof: We will split the proof in two parts, as follows:

1) For simplicity's sake, take $\boldsymbol{K}_{\text{pm}} = k_{\text{pm}}\boldsymbol{I}$, $\boldsymbol{K}_{\text{ps}} = k_{\text{ps}}\boldsymbol{I}$, $\boldsymbol{K}_{\text{vm}} = k_{\text{vm}}\boldsymbol{I}$, and $\boldsymbol{K}_{\text{vs}} = k_{\text{vs}}\boldsymbol{I}$ in (22) and (23). Let us decompose the dynamics given by (34), (35), and (38) into two parts, i.e.,

$$\dot{\boldsymbol{x}} = \boldsymbol{f}_u + \boldsymbol{f}_f \tag{46}$$

where $\boldsymbol{f}_u$ denotes the unforced part of the dynamics, given by $\boldsymbol{f}_u \triangleq \left[(\boldsymbol{q}_{2\,m} - \boldsymbol{q}_{2\,s})\ \boldsymbol{f}_{u2\,m}\ \boldsymbol{f}_{u2\,s}\ \boldsymbol{f}_{\text{uok}}\right]^T$, with

$$\boldsymbol{f}_{u2\,m} = \boldsymbol{H}_m^{-1}(\boldsymbol{q}_{1\,m})\big(-k_{\text{vm}}\boldsymbol{q}_{2m} - k_{\text{pm}}\boldsymbol{e} - \boldsymbol{C}_m(\boldsymbol{q}_{1\,m}, \boldsymbol{q}_{2\,m})\boldsymbol{q}_{2\,m}\big) \tag{47}$$

$$\boldsymbol{f}_{u2\,s} = \boldsymbol{H}_s^{-1}(\boldsymbol{q}_{1\,s})\big(-k_{\text{vs}}\boldsymbol{q}_{2\,s} + k_{\text{ps}}\boldsymbol{e} - \boldsymbol{C}_s(\boldsymbol{q}_{1\,s}, \boldsymbol{q}_{2\,s})\boldsymbol{q}_{2\,s}\big) \tag{48}$$

$$\boldsymbol{f}_{\text{uok}} = \boldsymbol{A}_{\text{ok}}\boldsymbol{x}_{\text{ok}} \tag{49}$$

with $\boldsymbol{A}_{\text{ok}}$ defined in (39). In turn, $\boldsymbol{f}_f$ represents the forced part of the closed-loop dynamics, which is bounded in $\mathcal{B}_r$ after Lemma 1, and is given by $\boldsymbol{f}_f \triangleq \left[\boldsymbol{0}\ \ \boldsymbol{f}_{f2\,m}\ \ \boldsymbol{f}_{f2\,s}\ \ \boldsymbol{f}_{\text{fok}}\right]^T$, where

$$\boldsymbol{f}_{f2\,m} = \boldsymbol{H}_m^{-1}(\boldsymbol{q}_{1\,m}) \times \Big(\boldsymbol{K}_{\text{vm}}\tilde{\boldsymbol{q}}_{2\,m} + \boldsymbol{\tau}_h - \boldsymbol{\tau}_e(t - T_s) + \tilde{\boldsymbol{\tau}}_e(t - T_s) + \boldsymbol{K}_{\text{pm}}\int_{t-T_s}^{t}\boldsymbol{q}_{2\,s}(\sigma)d\sigma\Big) \tag{50}$$

$$\boldsymbol{f}_{f2\,s} = \boldsymbol{H}_s^{-1}(\boldsymbol{q}_{1\,s})\Big(\boldsymbol{K}_{\text{vs}}\tilde{\boldsymbol{q}}_{2\,s} + \tilde{\boldsymbol{\tau}}_e + \boldsymbol{K}_{\text{ps}}\int_{t-T_m}^{t}\boldsymbol{q}_{2\,m}(\sigma)d\sigma\Big) \tag{51}$$

$$\boldsymbol{f}_{\text{fok}} = \boldsymbol{B}_{\text{ok}}\boldsymbol{u}_{\text{rfk}}. \tag{52}$$

Now, consider the positive definite function

$$V = \frac{k_{\text{ps}}}{2}\boldsymbol{q}_{2\,m}^T\boldsymbol{H}_m(\boldsymbol{q}_{1\,m})\boldsymbol{q}_{2\,m} + \frac{k_{\text{pm}}}{2}\boldsymbol{q}_{2\,s}^T\boldsymbol{H}_s(\boldsymbol{q}_{1\,s})\boldsymbol{q}_{2\,s} + \frac{k_{\text{pm}}k_{\text{ps}}}{2}\boldsymbol{e}^T\boldsymbol{e} + \boldsymbol{x}_{\text{om}}^T\boldsymbol{P}_{\text{om}}\boldsymbol{x}_{\text{om}} + \boldsymbol{x}_{\text{os}}^T\boldsymbol{P}_{\text{os}}\boldsymbol{x}_{\text{os}}. \tag{53}$$

The derivative of this function along the trajectories of the unforced system ($\boldsymbol{f}_f = \boldsymbol{0}$) is given by

$$\begin{aligned}\dot{V} = {} & k_{\text{ps}}\boldsymbol{q}_{2\,m}^T(-k_{\text{vm}}\boldsymbol{q}_{2\,m} - k_{\text{pm}}\boldsymbol{e}) \\ & + k_{\text{pm}}\boldsymbol{q}_{2\,s}^T(-k_{\text{vs}}\boldsymbol{q}_{2\,s} + k_{\text{ps}}\boldsymbol{e}) \\ & + k_{\text{pm}}k_{\text{ps}}\boldsymbol{e}^T(\boldsymbol{q}_{2\,m} - \boldsymbol{q}_{2\,s}) \\ & + \boldsymbol{x}_{\text{om}}^T(\boldsymbol{A}_{\text{om}}^T\boldsymbol{P}_{\text{om}} + \boldsymbol{P}_{\text{om}}\boldsymbol{A}_{\text{om}})\boldsymbol{x}_{\text{om}} \\ & + \boldsymbol{x}_{\text{os}}^T(\boldsymbol{A}_{\text{os}}^T\boldsymbol{P}_{\text{os}} + \boldsymbol{P}_{\text{os}}\boldsymbol{A}_{\text{os}})\boldsymbol{x}_{\text{os}}\end{aligned} \tag{54}$$

where Property 2 has been employed. By simplifying terms, one has

$$\dot{V} = -k_{\text{ps}}k_{\text{vm}}\boldsymbol{q}_{2\,m}^T\boldsymbol{q}_{2\,m} - k_{\text{pm}}k_{\text{vs}}\boldsymbol{q}_{2\,s}^T\boldsymbol{q}_{2\,s} - \boldsymbol{x}_{\text{om}}^T\boldsymbol{Q}_{\text{om}}\boldsymbol{x}_{\text{om}} - \boldsymbol{x}_{\text{os}}^T\boldsymbol{Q}_{\text{os}}\boldsymbol{x}_{\text{os}} \le 0. \tag{55}$$

By applying LaSalle's invariance lemma, it is not difficult to see that the unforced system is asymptotically stable. A Lyapunov converse theorem [53, Th. 24, Ch. 5] can be applied, by considering Assumption 5, to show that there exist a C^k function V_a and class K functions α_1–α_3 such that

$$\alpha_1(\|\boldsymbol{x}\|) \le V_a(\boldsymbol{x}) \le \alpha_2(\|\boldsymbol{x}\|) \quad \forall t \ge t_0\ \forall \boldsymbol{x} \in \mathcal{B}_r \tag{56}$$

$$\dot{V}_a(\boldsymbol{x}) \le -\alpha_3(\|\boldsymbol{x}\|) \quad \forall t \ge t_0\ \forall \boldsymbol{x} \in \mathcal{B}_r \tag{57}$$

$$\sup_{\boldsymbol{x}\in\mathcal{B}_r}\left\|\frac{\partial V_a(\boldsymbol{x})}{\partial \boldsymbol{x}}\right\| < \infty. \tag{58}$$

Now, in [52, Lemma 9.2], the state $\boldsymbol{x}$ in (31) is ultimately bounded if the perturbation term, i.e., the forced part of the system, satisfies the uniform bound

$$\|\boldsymbol{f}_f\| \le \delta < \frac{\theta\alpha_3\big(\alpha_2^{-1}(\alpha_1(x_{\max}))\big)}{\alpha_4(x_{\max})} \tag{59}$$

for some positive constants $\delta > 0$ and $0 < \theta < 1$. From the definition of $\boldsymbol{f}_f$, it can be seen that these perturbation terms shrink when the external forces $\boldsymbol{\tau}_e$ and $\boldsymbol{\tau}_h$, and the time delays $T_m(t)$ and $T_s(t)$ are small. Thus, the result is valid only for sufficiently small external forces and time delays, meaning that the ultimate boundedness of the state is not satisfied for any bounded perturbation in the end despite its magnitude. This is because the unforced part of the system has been shown to be only asymptotically (but not exponentially) stable since V in (53) is not a strict Lyapunov function for the unforced part of the system.

2) By taking into account Assumption 3, $\boldsymbol{\tau}_h$ and $\boldsymbol{\tau}_e$ are bounded, so that as long as $\boldsymbol{x}$ stays in $\mathcal{B}_r = \{\boldsymbol{x} \in \mathbb{R}^{3n+2(p+2)} : \|\boldsymbol{x}(t)\| \le x_{\max}\}$, by Lemma 1, $\boldsymbol{q}_{2\,m}$, $\boldsymbol{q}_{2\,s}$, $\tilde{\boldsymbol{q}}_{2\,m}$, $\tilde{\boldsymbol{q}}_{2\,s}$, $\tilde{\boldsymbol{\tau}}_e$, $\boldsymbol{u}_{\text{rfs}}$, and $\boldsymbol{u}_{\text{rfm}}$ are bounded as well. Recall that just as mentioned at the end of item 1) of the proof, $x_{\max}$ cannot be chosen freely. Let us denote the bounds in $\mathcal{B}_r$, $c_{b2} \triangleq \max_{\mathcal{B}_r}\|\boldsymbol{q}_{2\,m}\|$, and $c_{b3} \triangleq \max_{\mathcal{B}_r}\|\boldsymbol{q}_{2\,s}\|$. By taking the derivative of V along the trajectories of (46), it is obtained that

$$\begin{aligned}\dot{V} = {} & -k_{\text{ps}}\boldsymbol{q}_{2\,m}^T\Big(k_{\text{vm}}\boldsymbol{q}_{2\,m} - k_{\text{vm}}\tilde{\boldsymbol{q}}_{2\,m} - \boldsymbol{\tau}_h + \boldsymbol{\tau}_e(t - T_s) - \tilde{\boldsymbol{\tau}}_e(t - T_s) - k_{\text{pm}}\int_{t-T_s}^{t}\boldsymbol{q}_{2\,s}(\sigma)d\sigma\Big) \\ & - k_{\text{pm}}\boldsymbol{q}_{2\,s}^T\Big(k_{\text{vs}}\boldsymbol{q}_{2\,s} - k_{\text{vs}}\tilde{\boldsymbol{q}}_{2\,s} - \tilde{\boldsymbol{\tau}}_e - k_{\text{ps}}\int_{t-T_m}^{t}\boldsymbol{q}_{2\,m}(\sigma)d\sigma\Big) \\ & - \boldsymbol{x}_{\text{om}}^T\boldsymbol{Q}_{\text{om}}\boldsymbol{x}_{\text{om}} \\ & - \boldsymbol{x}_{\text{os}}^T\boldsymbol{Q}_{\text{os}}\boldsymbol{x}_{\text{os}} + 2\boldsymbol{x}_{\text{om}}^T\boldsymbol{P}_{\text{om}}\boldsymbol{B}_{\text{om}}\boldsymbol{u}_{\text{rfm}} \\ & + 2\boldsymbol{x}_{\text{os}}^{\text{T}}\boldsymbol{P}_{\text{os}}\boldsymbol{B}_{\text{os}}\boldsymbol{u}_{\text{rfs}} \\ \le {} & -k_{\text{ps}}\|\boldsymbol{q}_{2m}\| \\ & \times\big(k_{\text{vm}}\|\boldsymbol{q}_{2m}\| - k_{\text{vm}}\|\tilde{q}_{2m}\| - \|\boldsymbol{\tau}_h - \boldsymbol{\tau}_e(t - T_s)\| - \|\tilde{\tau}_e\| - k_{\text{pm}}c_{b3}c_{\text{Ts}}\big) \\ & - k_{\text{pm}}\|\boldsymbol{q}_{2s}\|\end{aligned} \tag{60}$$

$$\times \left(k_{\rm vs}\|\boldsymbol{q}_{2s}\| - k_{\rm vs}\|\tilde{q}_{2s}\| - k_{\rm ps}c_{b2}c_{\rm Tm} - \|\tilde{\tau}_e\|\right) - \lambda_{\min}(\boldsymbol{Q}_{\rm om})\|\boldsymbol{x}_{\rm om}\| \times \left(\|\boldsymbol{x}_{\rm om}\| - 2\frac{\lambda_{\max}(\boldsymbol{P}_{\rm om})}{\lambda_{\min}(\boldsymbol{Q}_{\rm om})}\|u_{\rm rfm}\|\right) - \lambda_{\min}(\boldsymbol{Q}_{\rm os})\|\boldsymbol{x}_{\rm os}\|\left(\|\boldsymbol{x}_{\rm os}\| - 2\frac{\lambda_{\max}(\boldsymbol{P}_{\rm os})}{\lambda_{\min}(\boldsymbol{Q}_{\rm os})}\|u_{\rm rfs}\|\right). \tag{61}$$

Consequently, $\dot{V} \leq 0$ if

$$\|\boldsymbol{q}_{2m}\| \geq \|\tilde{q}_{2m}\| + \frac{c_1}{k_{\rm vm}} \tag{62}$$

$$\|\boldsymbol{q}_{2s}\| \geq \|\tilde{q}_{2s}\| + \frac{c_2}{k_{\rm vs}} \tag{63}$$

$$\|\boldsymbol{x}_{\rm om}\| \geq 2\frac{\lambda_{\max}(\boldsymbol{P}_{\rm om})}{\lambda_{\min}(\boldsymbol{Q}_{\rm om})}\|u_{\rm rfm}\| \tag{64}$$

$$\|\boldsymbol{x}_{\rm os}\| \geq 2\frac{\lambda_{\max}(\boldsymbol{P}_{\rm os})}{\lambda_{\min}(\boldsymbol{Q}_{\rm os})}\|u_{\rm rfs}\| \tag{65}$$

where

$$c_1 = \|\tau_h - \tau_e\| + \|\tilde{\tau}_e\| + k_{\rm pm}c_{b3}c_{\rm Ts} \tag{66}$$

$$c_2 = \|\tilde{\tau}_e\| + k_{\rm ps}c_{b2}c_{\rm Tm}. \tag{67}$$

Of all the right-hand side terms, $\|\tilde{q}_{2m}\|$, $\|\tilde{q}_{2s}\|$, and $\|\tilde{\tau}_e\|$, and the ratios $\lambda_{\max}(\boldsymbol{P}_{\rm om})/\lambda_{\min}(\boldsymbol{Q}_{\rm om})$ and $\lambda_{\max}(\boldsymbol{P}_{\rm os})/\lambda_{\min}(\boldsymbol{Q}_{\rm os})$ can be made arbitrarily small by tuning the observer gains properly. In turn, the terms c_1 and c_2 depend on external forces and time delays. From the above analysis, it is stated that $\boldsymbol{e}$ must be bounded in $\mathcal{B}_r$. Thus, the only possibility is that $\boldsymbol{q}_{2m}$ and $\boldsymbol{q}_{2s}$ tend to a region bounded by $\|\boldsymbol{q}_{2m}\| \leq \|\tilde{q}_{2m}\| + c_1/k_{\rm vm}$ and $\|\boldsymbol{q}_{2s}\| \leq \|\tilde{q}_{2s}\| + c_2/k_{\rm vs}$. As explained before, all the estimation error quantities, denoted by $\tilde{(\cdot)}$, can be made arbitrarily small as well by properly tuning the observer gains in (12)–(16), see Remark 3. Finally, the gains $k_{\rm vm}$ and $k_{\rm vs}$ can be tuned large to reduce the effects of c_1 and c_2 defined in (66) and (67).

■

The following remarks are useful to gain insight into the implementation of the proposed scheme.

Remark 4: While there is no problem in setting the observer gains very large, the controller derivative gains $k_{\rm vm}$ and $k_{\rm vs}$ are limited by the bandwidth of the system. Moreover, if these gains are large, the overall system could be stiff to the human operator. However, for the special case of no external forces, i.e., $\boldsymbol{\tau}_h = \boldsymbol{\tau}_e = \boldsymbol{0}$, the ultimate bound for the velocities can be shrunk, as can be seen in (62) and (63), by setting the ratios $k_{\rm pm}/k_{\rm vm}$ and $k_{\rm ps}/k_{\rm vs}$ small. □

Remark 5: In this work, we have chosen not to include the other robot velocity (nor its estimate) in their corresponding control laws, i.e., $\boldsymbol{\tau}_m$ does not depend on $\hat{\boldsymbol{q}}_{2s}$ and vice versa. Although the inclusion of such velocities is of great help when developing the stability proof, in practice, these terms are counterproductive and they are frequently dominated by including an extra term of local damping. By including only local damping, we have the additional advantage that fewer signals are transmitted through the communication channel (only the two positions and the estimated environmental force). □

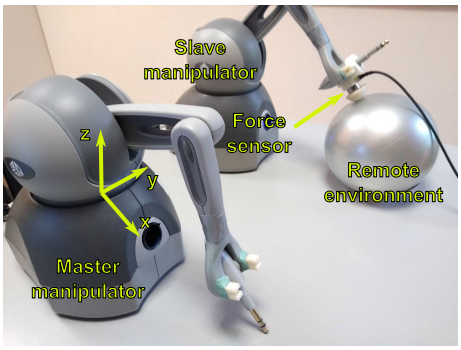

Fig. 2. Setup employed for the laboratory experiment.

IV. Experimental Results

The experimental setup consists of two 3D Systems Touch manipulators, as shown in Fig. 2. One of the robots is connected to the PC via Ethernet, while the other one is connected via USB. Both robots have similar mechanical characteristics, with a workspace resolution of approximately 0.055 mm and a maximum exertable force of 3.3 N. The robots were programmed by employing the OpenHaptics HDAPI running under Windows 10. Both robots are programmed in C++ language with Visual Studio C/C++. The sample time for the entire system is 2 ms, which is possible by implementing the Windows Multimedia Timers. As a part of the experimental data, a time vector is obtained, from which the sample time can be verified to have a mean of 2 ms. Thus, the sampling time and the quantization errors are not a problem for the implementation of the continuous controllers and observers designed in Section III. For experimental platforms with slower sampling times or large quantization errors, sufficient conditions for preserving the continuous system stability can be found in [54].

For all the experiments presented next, both manipulators are first driven to a home position by a standard PD controller, and then, the user switches to teleoperation mode. Only the first three joints of both manipulators are employed, while the remaining three are mechanically blocked. The dynamic model for the three degrees of freedom configuration of the Phantom Touch manipulator can be found in [45, Ch. 14], along with a linear parametrization, which was used to identify a new set of parameters due to the addition of the force sensor to the tip of the slave manipulator. The master robot is manipulated directly by the human operator, whereas the slave interacts with the remote surface. Two different scenarios were tested: in the first experiment, a rigid book is employed, whereas in the second experiment, a soft surface consisting of a softball used for yoga training serves as the remote surface.

A. Laboratory Experiment

In the following experiments, the user is intended to interact with the remote objects, i.e., a rigid book and a softball. Asymmetrical artificially created time-varying delays are included in both directions, i.e., a delay from master to slave signals T_m

taking random values in the interval [0.25, 0.35] s and a delay from slave to master signals T_s taking random values in the interval [0.2, 0.3] s.

1) Book Experiment: In this experiment, both robots start in free motion, while the user approaches the book. Once in contact with it, the operator exerts a force over it and intends to draw a circle over the book's surface. After three circles, the user enters again in free motion, and then, he tries to rotate the book by exerting a force over one of its corners. Finally, the user exerts force over another corner to rotate the book in the opposite direction.

2) Ball Experiment: In this experiment, both robots start in free motion again, and the user approaches the ball. Once in contact with it, the operator pushes it and tries to move the ball in circles, first in one direction and then in the opposite one.

A video of these two experiments is available at https://youtu.be/I-auZqvtdIc.

Tuning Procedure:

1) The observer gains in (12)–(16) can be set by choosing the roots of the polynomials in (37) as far in the left-hand side of the complex plane as allowed by the system bandwidth.
2) The controller gains $\boldsymbol{K}_{\mathrm{pm}}$ and $\boldsymbol{K}_{\mathrm{vm}}$ for the master controller (22), and $\boldsymbol{K}_{\mathrm{ps}}$ and $\boldsymbol{K}_{\mathrm{vs}}$ for the slave controller (23) can be set by standard PD tuning methods. If better performance is wanted, some techniques for PD tuning can be applied by taking advantage of the dynamic model knowledge (e.g., [48, p. 213]).
3) To deal with noise effects, first-order filters can be used to obtain the velocity and force signals employed in the control laws (22) and (23).

For both observers, the degree of the polynomial (37), $p = 2$ is chosen. The observer gains in (12)–(16) were set to $\lambda_{0m} = \lambda_{0s} = 1 \times 10^8 \boldsymbol{I}$, $\lambda_{1m} = \lambda_{1s} = 4 \times 10^6 \boldsymbol{I}$, $\lambda_{2m} = \lambda_{2s} = 6 \times 10^4 \boldsymbol{I}$, and $\lambda_{3m} = \lambda_{3s} = 400\boldsymbol{I}$, i.e., the observer poles were located at $p_1 = p_2 = p_3 = p_4 = -100$ for both robots. The controller gains for the master manipulator in (22) are chosen as $\boldsymbol{K}_{\mathrm{pm}} = 0.001\boldsymbol{I}$ and $\boldsymbol{K}_{\mathrm{vm}} = 0.001\boldsymbol{I}$, whereas the gains for the slave controller (23) are $\boldsymbol{K}_{\mathrm{ps}} = 2.0\boldsymbol{I}$ and $\boldsymbol{K}_{\mathrm{vs}} = 0.02\boldsymbol{I}$. First-order filters with a cutoff frequency of 10 Hz were used for the velocity and force signals employed in the control laws (22) and (23).

Although all the controllers and observers were implemented in joint coordinates, the results are presented in Cartesian coordinates, obtained from direct kinematics, i.e., $\begin{bmatrix} x_k & y_k & z_k \end{bmatrix}^T = \boldsymbol{f}_{\mathrm{DK}}(\boldsymbol{q}_{1k})$. Similarly, the contact forces are expressed in the Cartesian base frame by using the well-known relationship $\boldsymbol{\tau} = \boldsymbol{J}(\boldsymbol{q})^T \boldsymbol{F}$, where $\boldsymbol{J}(\boldsymbol{q})$ is the manipulator Jacobian.

Remark 6: If a peaking phenomenon, which commonly arises when employing high-gain observers, is presented, a suitable clutch can be implemented at the start of the robot motion, as explained in [47]. □

The time evolution of the Cartesian coordinates for both master and slave robots for the book experiment is shown in Fig. 3. The estimated Cartesian velocities for both robots are shown in Fig. 4. The Cartesian forces measured at the slave side, along with the estimated forces at the master and the slave sides, are shown in Fig. 5.

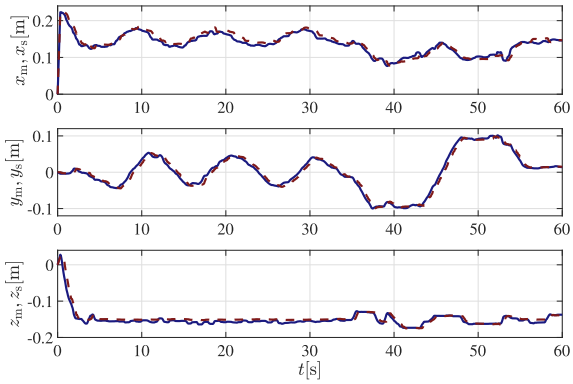

Fig. 3. Book experiment, the proposed scheme: time evolution of the Cartesian coordinates of master (—) and slave (- - -) robots.

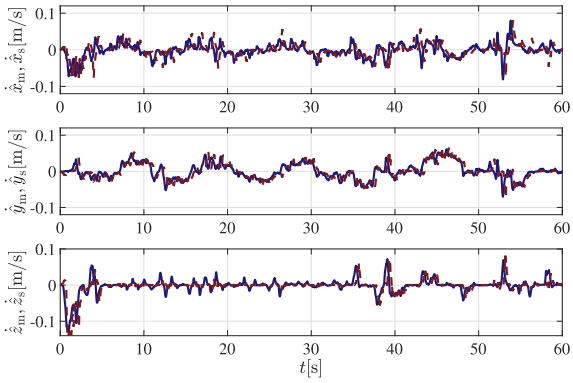

Fig. 4. Book experiment, the proposed scheme: estimated Cartesian velocities of master (—) and slave (- - -) robots.

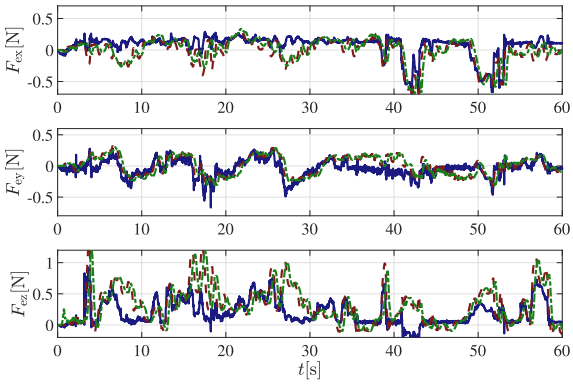

Fig. 5. Book experiment, the proposed scheme: Cartesian forces measured at the slave side (—), estimated at the slave side (- - -), and estimated at the master side (- · -).

B. Comparative Experiment

In this section, a comparison of the proposed scheme with one relatively recent result published in [40] is presented, namely, the dynamic-gain ESO (DGESO). This scheme was chosen because of the similar design considerations shared with the proposed scheme: 1) only position is measured; 2) forces and velocities are estimated; and 3) time-varying delays are considered in the communication channel.

The DGESO was tuned by considering the constraints mentioned in the cited paper. Notice that the DGESO also requires a dynamic model of the manipulators. Although it

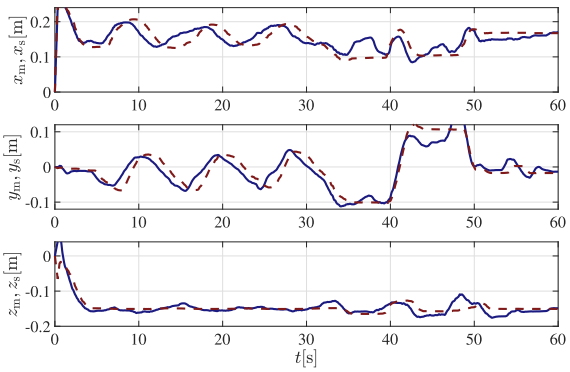

Fig. 6. Book experiment, DGESO: time evolution of the Cartesian coordinates of master (—) and slave (- - -) robots.

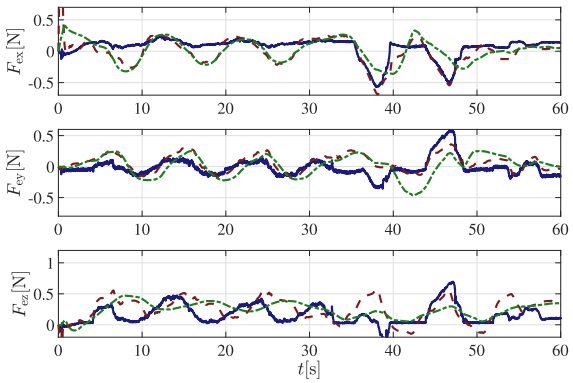

Fig. 7. Book experiment, DGESO: Cartesian forces measured at the slave side (—), estimated at the slave side (- - -), and estimated at the master side (- · -).

includes an adaptation algorithm, the performance is better if the parameters are initialized with those obtained by an offline identification.

For the observer part of the DGESO, the same gains of the original article were employed, i.e., parameters $\beta_{i1} = \text{diag}\{60, 60, 60\}$, $\beta_{i2} = \text{diag}\{440, 440, 440\}$, $\beta_{i3} = \text{diag}\{900, 900, 900\}$, $\alpha = 200$, $\lambda_{\max}(P_i) = 1.5$, $\mu_{ik}(t) = (0.6 - 0.01)e^{-2t} + 0.01$, $\underline{\delta}_{ik} = \overline{\delta}_{ik} = 2$, and $\psi_i = 0.01\boldsymbol{I}$. Such an election was possible due to the independence of these parameters on the robot dynamics. For tuning the controller parameters, we have proceeded as follows: first, we have set the wave transformation variables $b_1 = b_2 = 2$ as in the original paper and tuning $\lambda_1 = \lambda_2 = 3$, by trial and error until obtaining satisfactory performance. The parameters $\zeta_m = \zeta_s = 0.2$ were chosen as in the original version. The parameter $\gamma_1 = 0.01$ is related to local damping and therefore was chosen as half of K_{vs} of the proposed approach. The parameters $k_{m1} = k_{s1} = 1$ were set to satisfy [40, Remark 5, eqs. (65) and (66)]. The $\gamma_2 = 0.15$ parameter is related to the position error and was set by trial and error. Finally, the α_1 and α_2 parameters must satisfy [40, eq. (64)] and were originally set to $\alpha_1 = \alpha_2 = 0.7$ for the maximum delay of 0.35 s considered in the experiment. However, this setting leads to very stiff behavior and poor performance. Since conditions [40, eq. (64)] are very conservative and by looking at control laws [40, eqs. (58) and (59)], one can see that these gains are directly related to damping addition. Therefore, we have decided to reduce these gains to improve the performance at the expense of not satisfying conditions [40, eq. (64)], leading to $\alpha_1 = \alpha_2 = 0.02$. Notice that this is the only nonsatisfied condition given in [40], and this election could explain why with the same tuning it is not possible to deal with larger delays, as will be seen in Section IV-C.

The time evolution of the Cartesian coordinates for the DGESO approach, for both the master and the slave manipulators, is shown in Fig. 6. In turn, the estimated forces at the master and the slave sides, along with the measured force at the slave side are shown in Fig. 7.

The two experiments described in Section IV-A were considered for the comparison. Note that, since there is a human operator in the loop, the exact experiment cannot be repeated for each scheme exactly. To make the comparison study more reliable, each experiment was repeated ten times for each scheme, alternating between them.

TABLE I
BOOK EXPERIMENT: AVERAGE RMSE OF TEN EXPERIMENTS

Average RMSE	Proposed	DGESO
$x_m - x_s$ [mm]	9.2	22.3
$y_m - y_s$ [mm]	2.9	15.6
$z_m - z_s$ [mm]	8.1	14.1
$F_{ex} - \hat{F}_{ex}$ [N]	0.1884	0.2038
$F_{ey} - \hat{F}_{ey}$ [N]	0.1175	0.1463
$F_{ez} - \hat{F}_{ez}$ [N]	0.3060	0.2445
$\hat{F}_{hx} - \hat{F}_{ex}$ [N]	0.0748	0.1627
$\hat{F}_{hy} - \hat{F}_{ey}$ [N]	0.0388	0.1142
$\hat{F}_{hz} - \hat{F}_{ez}$ [N]	0.0828	0.1594

TABLE II
BALL EXPERIMENT: AVERAGE RMSE OF TEN EXPERIMENTS

Average RMSE	Proposed	DGESO
$x_m - x_s$ [mm]	7.6	15.6
$y_m - y_s$ [mm]	2.7	24.1
$z_m - z_s$ [mm]	15.2	20.2
$F_{ex} - \hat{F}_{ex}$ [N]	0.1426	0.4686
$F_{ey} - \hat{F}_{ey}$ [N]	0.1048	0.0839
$F_{ez} - \hat{F}_{ez}$ [N]	0.1321	0.1877
$\hat{F}_{hx} - \hat{F}_{ex}$ [N]	0.0713	0.3825
$\hat{F}_{hy} - \hat{F}_{ey}$ [N]	0.0362	0.0531
$\hat{F}_{hz} - \hat{F}_{ez}$ [N]	0.0372	0.1249

To obtain an objective comparison, a quantitative analysis of the data is presented in Tables I and II. In Tables I and II, the average of the root-mean-square errors (RMSEs) of all ten experiment data signals both for the book and the ball experiments, for each scheme, is presented. The RMSE is defined as

$$\text{RMSE}(x) = \sqrt{\frac{\sum_{i=1}^{N_s} x_i^2}{N_s}} \tag{68}$$

where N_s is the sample size of each signal. An interpretation of the results of Tables I and II will be given in Section IV-E.

C. Effect of the Time Delay on the Performance

To obtain a measure of the effects of the time-delay magnitude on the performance of the above schemes, another experiment was carried out. This experiment consisted in increasing the time delay while preserving the same tuning

TABLE III
PROPOSED SCHEME: AVERAGE RMSE AS INCREASING THE TIME DELAY FOR THE BOOK EXPERIMENT

Time-delays ± 20 ms	80	160	320	640	1280	2560
$x_m - x_s$ [mm]	6.6	7.8	8.9	9.5	9.8	11.9
$y_m - y_s$ [mm]	2.4	2.7	3.3	2.9	3.3	3.1
$z_m - z_s$ [mm]	5.8	7.4	8.6	8.9	11.2	11.1
$F_{ex} - \hat{F}_{ex}$ [N]	0.19	0.21	0.24	0.26	0.34	0.26
$F_{ey} - \hat{F}_{ey}$ [N]	0.10	0.13	0.14	0.14	0.27	0.26
$F_{ez} - \hat{F}_{ez}$ [N]	0.27	0.41	0.52	0.56	0.98	0.79
$\hat{F}_{hx} - \hat{F}_{ex}$ [N]	0.05	0.09	0.08	0.13	0.27	0.29
$\hat{F}_{hy} - \hat{F}_{ey}$ [N]	0.03	0.06	0.05	0.08	0.16	0.20
$\hat{F}_{hz} - \hat{F}_{ez}$ [N]	0.07	0.13	0.11	0.11	0.11	0.08

TABLE IV
DGESO: AVERAGE RMSE AS INCREASING THE TIME DELAY FOR THE BOOK EXPERIMENT

Time-delay ± 20 ms	80	160	320	640	1280	2560
$x_m - x_s$ [mm]	15.6	18.5	21.8	–	–	–
$y_m - y_s$ [mm]	20.2	24.9	31.0	–	–	–
$z_m - z_s$ [mm]	8.0	8.6	9.2	–	–	–
$F_{ex} - \hat{F}_{ex}$ [N]	0.22	0.26	0.33	–	–	–
$F_{ey} - \hat{F}_{ey}$ [N]	0.13	0.11	0.10	–	–	–
$F_{ez} - \hat{F}_{ez}$ [N]	0.19	0.24	0.27	–	–	–
$\hat{F}_{hx} - \hat{F}_{ex}$ [N]	0.11	0.17	0.29	–	–	–
$\hat{F}_{hy} - \hat{F}_{ey}$ [N]	0.08	0.08	0.09	–	–	–
$\hat{F}_{hz} - \hat{F}_{ez}$ [N]	0.13	0.15	0.15	–	–	–

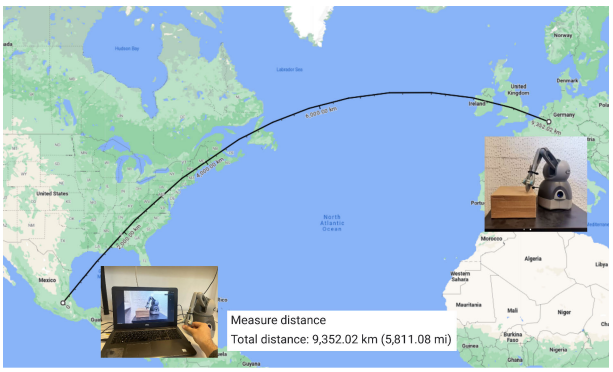

Fig. 8. Teleoperation through the Internet: location of the connection points. Approximate distance: 9352 km.

as in the experiments above. The user is asked to perform the experiment with the rigid book, without a time limit, as long as the manipulators remain stable and he feels comfortable with the task. The time delays for this experiment were symmetric, i.e., $T_m(t) = T_s(t)$ with increasing magnitude and the same variation of ± 20 ms. The results of this experiment are shown in Table III for the proposed approach and in Table IV for the DGESO. For the latter, the last three columns contain no data due to the instability of the approach with the same tuning.

D. Teleoperation Through the Internet

To test the performance of the proposed approach for time-varying delays under more realistic conditions, we carried out an experiment at two geographically distant points through the Internet. One robot was located at the Chair of Medical Engineering, Helmholtz Institute for Biomedical Engineering, RWTH Aachen University, Aachen, Germany, and the other one at the Mechatronics Section, Cinvestav, Mexico City,

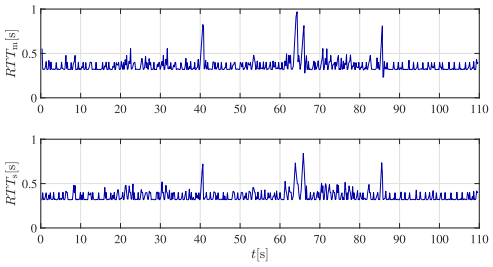

Fig. 9. Teleoperation through the Internet: RTT delay measured from the master side RTT_m (top) and the slave side RTT_s (bottom).

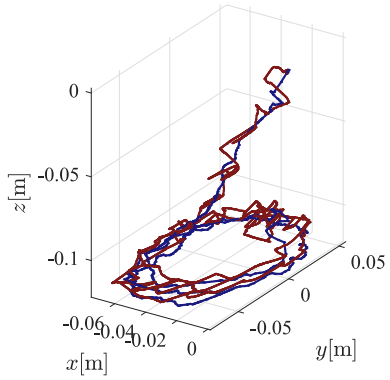

Fig. 10. Teleoperation through the Internet: 3-D trajectories of master (—) and slave (—) robots.

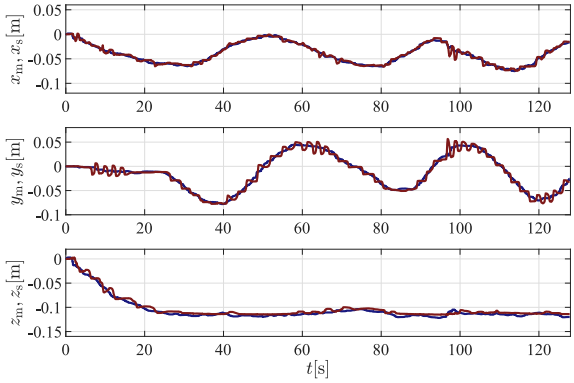

Fig. 11. Teleoperation through the Internet: time evolution of the Cartesian coordinates of master (—) and slave (—).

Mexico. The distance between these two locations is approximately 9352 km, as shown in Fig. 8. We employed Windows Sockets under the TCP/IP protocol to transfer the data. In this case, the sample time is incremented to $T = 3$ ms for both robots. Moreover, since the control system is decentralized, there is no necessity to transmit all signals, but only the positions $\boldsymbol{q}_{1m}$ and $\boldsymbol{q}_{1s}$ and estimated torques $\hat{\boldsymbol{\tau}}_h$ and $\hat{\boldsymbol{\tau}}_e$. The round trip time (RTT) communication delays measured from the data saved at the master and the slave sides are shown in Fig. 9. The RTT measured from the master side has a mean of 0.355 s, a standard deviation of 0.070 s, and a maximum value of 0.840 s. In turn, the RTT measured from the slave side has a mean of 0.356 s, a standard deviation of 0.061 s, and a maximum value of 0.969 s. As discussed recently in [55], the RTT is one of the most reliable parameters in evaluating bilateral teleoperation performance under time-varying delays. As a result of a practical limitation, for this case, downsampling of 1/50 is implemented on the transmitted signals to prevent any blocking or buffer saturations. All the observers and controller gains are the same as in the laboratory

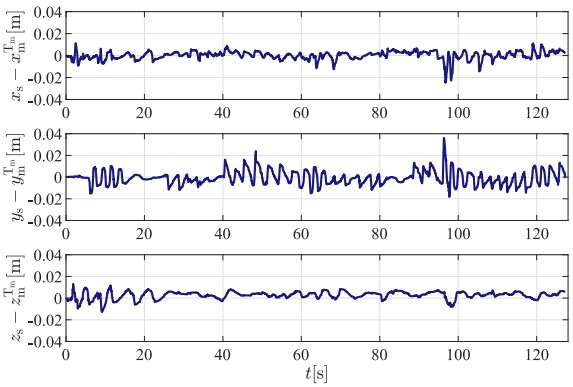

Fig. 12. Teleoperation through the Internet: time-adjusted Cartesian errors $\boldsymbol{x}_{1s} - \boldsymbol{x}_{1m}(t - T_m)$.

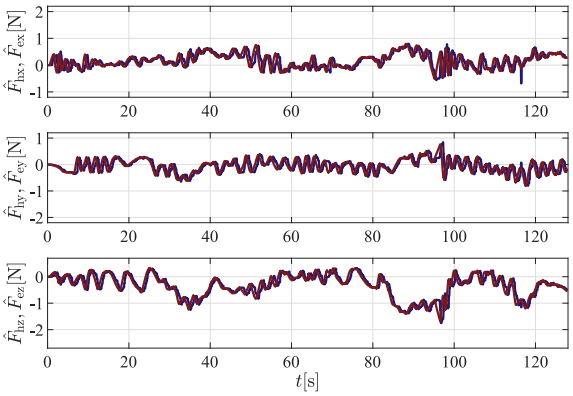

Fig. 13. Teleoperation through the Internet: estimated Cartesian forces of the human $\hat{F}_h$ (—) and the environment $\hat{F}_e$ (—).

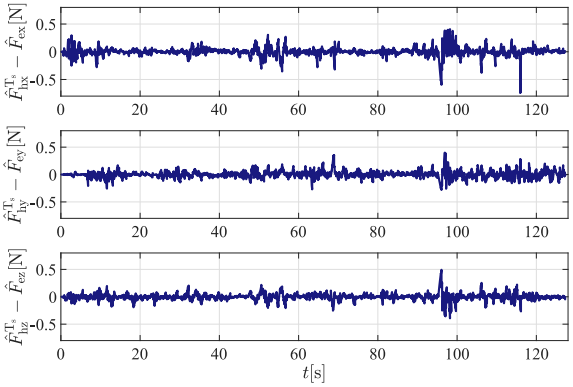

Fig. 14. Teleoperation through the Internet: the difference between estimated Cartesian forces at the master and slave sides.

experiment. For the experiments of this section, no force sensor validation is presented, due to the lack of a force sensor at the slave side. Nevertheless, we rely on the good results of Sections IV-A and IV-B to assume that the estimated forces are close to the real ones.

For the first experiment, the user intends to follow a circular trajectory over a flat surface while exerting a force on it. A 3-D plot of the trajectories in Cartesian coordinates for both robots is shown in Fig. 10. The time evolution of these coordinates is presented in Fig. 11, with their time-adjusted differences, i.e., $\boldsymbol{x}_{1s} - \boldsymbol{x}_{1m}^{T_m}$, shown in Fig. 12, where $\boldsymbol{x}_{1m}^{T_m} \triangleq \boldsymbol{x}_{1m}(t - T_m)$. Next, the estimation of the external forces $\hat{\boldsymbol{F}}_h$ and $\hat{\boldsymbol{F}}_e$ is shown in Fig. 13, whereas their time-adjusted differences, $\hat{\boldsymbol{F}}_h - \hat{\boldsymbol{F}}_e^{T_s}$, are shown in Fig. 14, where $\hat{\boldsymbol{F}}_e^{T_s} \triangleq \hat{\boldsymbol{F}}_e(t - T_s)$. This time adjustment is carried out by saving a file on each side, which

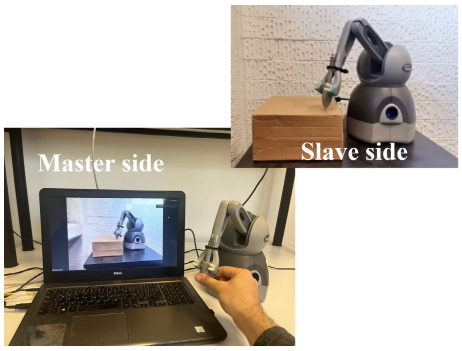

Fig. 15. Setup at the master and slave sides for the second Internet experiment.

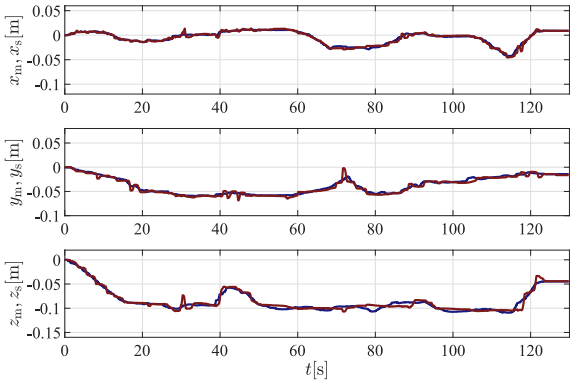

Fig. 16. Teleoperation through the Internet: time evolution of the Cartesian coordinates of master (—) and slave (—) robots.

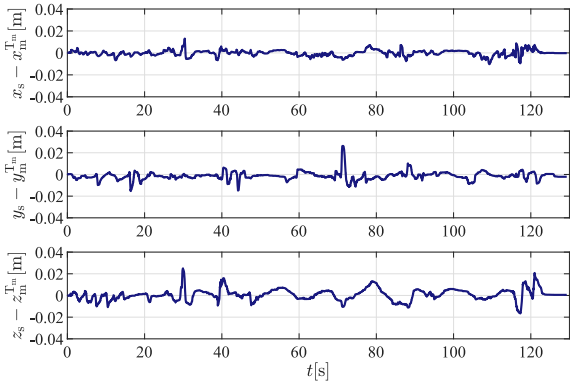

Fig. 17. Teleoperation through the Internet: time-adjusted Cartesian errors $\boldsymbol{x}_{1s} - \boldsymbol{x}_{1m}(t - T_m)$.

contains local and remote signals. Thus, at the slave side, one has $\boldsymbol{x}_{1s}(t)$ and $\boldsymbol{x}_{1m}(t - T_m)$, and at the master side, one has $\hat{\boldsymbol{F}}_h(t)$ and $\hat{\boldsymbol{F}}_e(t - T_s)$.

In the second experiment, the operator is asked to move a small cardboard filled with a load weight of approximately 0.2 kg as the one shown in Fig. 15. The time evolution of the Cartesian coordinates is shown in Fig. 16, whereas their time adjusted errors, $\boldsymbol{x}_{1s} - \boldsymbol{x}_{1m}^{T_m}$, are shown in Fig. 17. Finally, the estimated human $\hat{\boldsymbol{F}}_h$ and environment $\hat{\boldsymbol{F}}_e$ forces are shown in Fig. 18, along with their time adjusted differences, $\hat{\boldsymbol{F}}_h - \hat{\boldsymbol{F}}_e^{T_s}$, shown in Fig. 19.

E. Discussion

In the laboratory experiment of Section IV-A, the artificially created time delay makes it difficult for the user to carry out the intended task. Nevertheless, the position errors remain close to zero and below 20 mm in each coordinate during the

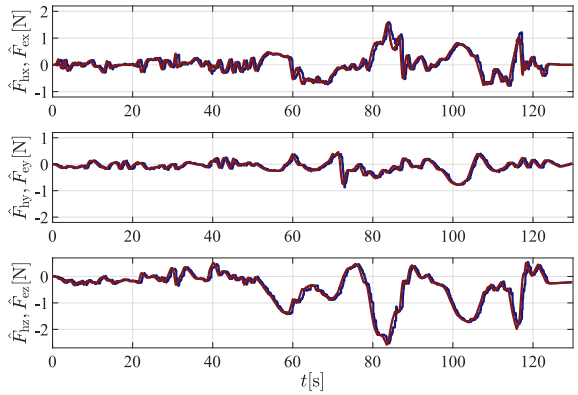

Fig. 18. Teleoperation through the Internet: estimated Cartesian forces of the human $\hat{F}_h$ (—) and the environment $\hat{F}_e$ (—).

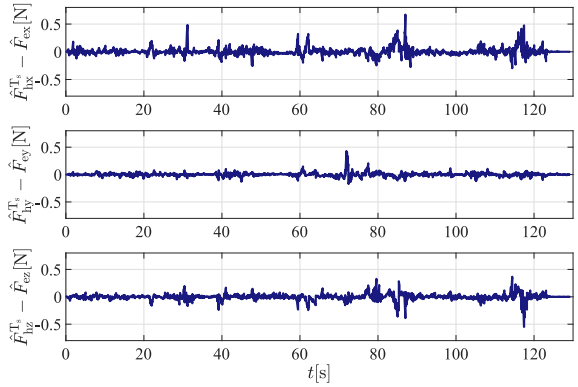

Fig. 19. Teleoperation through the Internet: time-adjusted differences between estimated forces at the master and slave sides.

whole experiment. In this experiment, it can be seen that the estimated and measured forces on the slave side are close to each other. As the velocities are estimated and employed only locally by the controllers, i.e., they are not transmitted through the communication channel, a good performance is expected, as shown in Fig. 4.

The comparison study presented in Section IV-B illustrates the performance of the proposed approach with respect to a relatively recent scheme taken from the literature (DGESO). Since the execution of the task involves a human operator, the experiment was repeated alternately ten times for each experiment and each of the schemes to make the comparison more reliable. The mean value of the RMSE indexes corresponding to all the experiments was then obtained as a measure of performance. These results are shown in Tables I and II. The results presented in Tables I and II show that though the force estimation performance is similar for both approaches, the proposed in this work outperforms the ESO in position tracking and force reflection, which are the main goals for a transparent teleoperation scheme. Moreover, the proposed approach is easier to implement than DGESO.

In the experiments of Section IV-D, we tested the validity of the assumptions on a real-case scenario, i.e., communication over a long distance by a common Internet protocol. The position tracking errors, although centered at zero, are not as good as in the first experiment. This is due to the necessity of the implementation of downsampling on the transmitted signals by 1/50, which is necessary to prevent buffer saturations and blocking in the sockets employed to make the communication. Another practical limitation is the visual feedback. In the laboratory experiment, with a similar time delay, the visual feedback to the user is not delayed and he/she is able to correct or even, after some trials, develop a strategy to better perform the task. In contrast, for the real-case scenario, the visual feedback is delayed even more than the transmitted position and force signals. Although the performance is not as good as in the first experiment, the position errors also remain close to zero. In the same form, the difference between the estimated torques is always close to zero.

V. Conclusion

This work proposes an observer-based controller for robotic teleoperation by using only joint position measurements. The proposed controller–observer is designed to be easy to implement. A formal mathematical analysis carried out in this article guarantees the convergence to an arbitrarily small ultimate bound of the observation error signals and robot velocities. The proposed scheme also provides an arbitrarily close estimation of the human and environmental forces. Moreover, the human and environmental forces difference is arbitrarily small, which can be transferred to the telepresence of the human operator. The experiments presented in this work validate the good performance of the proposed approach, both when compared with an already available scheme in the literature and in a real scenario in an intercontinental teleoperation experiment through the Internet. In all the experiments, the proposed scheme shows good position tracking, force reflection, and force estimation.

In future work, practical limitations, such as buffer saturations and efficiency of the communication protocols, will be investigated to improve the controller–observer design. From a theoretical point of view, stronger stability conditions will be pursued either by finding a strict Lyapunov function for the closed-loop analysis presented in this work or by exploring an alternative way to perform the stability proof. In addition, the analysis and design of a controller–observer for time-delayed teleoperation in the Hamiltonian framework will be studied.

References

[1] R. C. Goertz, *Mechanical Master-Slave Manipulator*, vol. 12. Lemont, IL, USA: Argonne National Lab., Nucleonics (US) Ceased, 1954.

[2] R. J. Anderson and M. W. Spong, "Bilateral control of teleoperators with time delay," *IEEE Trans. Autom. Control*, vol. 34, no. 5, pp. 494–501, May 1989.

[3] G. Niemeyer and J.-J. E. Slotine, "Stable adaptive teleoperation," *IEEE J. Ocean. Eng.*, vol. 16, no. 1, pp. 152–162, Jan. 1991.

[4] S. N. F. Nahri, S. Du, and B. J. Van Wyk, "A review on haptic bilateral teleoperation systems," *J. Intell. Robotic Syst.*, vol. 104, no. 1, pp. 1–23, Jan. 2022.

[5] E. Nuño, L. Basañez, and R. Ortega, "Passivity-based control for bilateral teleoperation: A tutorial," *Automatica*, vol. 47, no. 3, pp. 485–495, Mar. 2011.

[6] O. Kostyukova, F. P. Vista, and K. T. Chong, "Design of feedforward and feedback position control for passive bilateral teleoperation with delays," *ISA Trans.*, vol. 85, pp. 200–213, Feb. 2019.

[7] M. Namnabat, A. H. Zaeri, and M. Vahedi, "A passivity-based control strategy for nonlinear bilateral teleoperation employing estimated external forces," *J. Brazilian Soc. Mech. Sci. Eng.*, vol. 42, no. 12, pp. 1–10, Nov. 2020.

[8] M. Mattioni, A. Moreschini, S. Monaco, and D. Normand-Cyrot, "Reduction-based stabilization of nonlinear discrete-time systems through delayed state measurements," *IFAC-PapersOnLine*, vol. 53, no. 2, pp. 5851–5856, 2020.

[9] Y. Zhu, T. Aoyama, and Y. Hasegawa, "Enhancing the transparency by onomatopoeia for passivity-based time-delayed teleoperation," *IEEE Robot. Autom. Lett.*, vol. 5, no. 2, pp. 2981–2986, Apr. 2020.

[10] I. Sharifi, H. A. Talebi, and M. Motaharifar, "Robust output feedback controller design for time-delayed teleoperation: Experimental results," *Asian J. Control*, vol. 19, no. 2, pp. 625–635, Mar. 2017.

[11] M. Sharifi, H. Salarieh, S. Behzadipour, and M. Tavakoli, "Impedance control of non-linear multi-DOF teleoperation systems with time delay: Absolute stability," *IET Control Theory Appl.*, vol. 12, no. 12, pp. 1722–1729, Aug. 2018.

[12] L. Zhao, H. Zhang, Y. Yang, and H. Yang, "Integral sliding mode control of a bilateral teleoperation system based on extended state observers," *Int. J. Control, Autom. Syst.*, vol. 15, no. 5, pp. 2118–2125, Oct. 2017.

[13] B. Aboutalebian, H. A. Talebi, S. Etedali, and A. A. Suratgar, "Adaptive control of teleoperation system based on nonlinear disturbance observer," *Eur. J. Control*, vol. 53, pp. 109–116, May 2020.

[14] S. Hao, L. Hu, and P. X. Liu, "Sliding mode control for a surgical teleoperation system via a disturbance observer," *IEEE Access*, vol. 7, pp. 43383–43393, 2019.

[15] S. Shen, A. Song, T. Li, and H. Li, "Time delay compensation for nonlinear bilateral teleoperation: A motion prediction approach," *Trans. Inst. Meas. Control*, vol. 41, no. 16, pp. 4488–4498, Dec. 2019.

[16] J. Tang, F. Huang, Z. Chen, T. Wang, J. Gu, and S. Zhu, "Disturbance-observer-based sliding mode control design for nonlinear bilateral teleoperation system with four-channel architecture," *IEEE Access*, vol. 7, pp. 72672–72683, 2019.

[17] L. Chan, Q. Huang, and P. Wang, "Adaptive-observer-based robust control for a time-delayed teleoperation system with scaled four-channel architecture," *Robotica*, vol. 40, no. 5, pp. 1385–1405, May 2022.

[18] M. V. de Lima, L. A. Mozelli, A. A. Neto, and F. O. Souza, "A simple algebraic criterion for stability of bilateral teleoperation systems under time-varying delays," *Mech. Syst. Signal Process.*, vol. 137, Mar. 2020, Art. no. 106217.

[19] R. Balachandran, J.-H. Ryu, M. Jorda, C. Ott, and A. Albu-Schaeffer, "Closing the force loop to enhance transparency in time-delayed teleoperation," in *Proc. IEEE Int. Conf. Robot. Autom. (ICRA)*, Paris, France, May 2020, pp. 10198–10204.

[20] P. N. Dao, V. T. Nguyen, and Y. Liu, "Finite-time convergence for bilateral teleoperation systems with disturbance and time-varying delays," *IET Control Theory Appl.*, vol. 15, no. 13, pp. 1736–1748, Sep. 2021.

[21] Y. Wang et al., "Adaptive neural network control of time delay teleoperation system based on model approximation," *Sensors*, vol. 21, no. 22, p. 7443, Nov. 2021.

[22] S. Zhang, S. Yuan, X. Yu, L. Kong, Q. Li, and G. Li, "Adaptive neural network fixed-time control design for bilateral teleoperation with time delay," *IEEE Trans. Cybern.*, vol. 52, no. 9, pp. 9756–9769, Sep. 2022.

[23] D. A. Lawrence, "Stability and transparency in bilateral teleoperation," *IEEE Trans. Robot. Autom.*, vol. 9, no. 5, pp. 624–637, Oct. 1993.

[24] Z. Lu, P. Huang, and Z. Liu, "High-gain nonlinear observer-based impedance control for deformable object cooperative teleoperation with nonlinear contact model," *Int. J. Robust Nonlinear Control*, vol. 30, no. 4, pp. 1329–1350, Mar. 2020.

[25] M. Laghi, A. Ajoudani, M. G. Catalano, and A. Bicchi, "Unifying bilateral teleoperation and tele-impedance for enhanced user experience," *Int. J. Robot. Res.*, vol. 39, no. 4, pp. 514–539, Mar. 2020.

[26] X. Gong et al., "Improved four-channel PBTDPA control strategy using force feedback bilateral teleoperation system," *Int. J. Control, Autom. Syst.*, vol. 20, no. 3, pp. 1002–1017, Mar. 2022.

[27] N. Piccinelli and R. Muradore, "A bilateral teleoperation with interaction force constraint in unknown environment using non linear model predictive control," *Eur. J. Control*, vol. 62, pp. 185–191, Nov. 2021.

[28] U. Tumerdem and N. Yilmaz, "A unifying framework for transparency optimized controller design in multilateral teleoperation with time delays," *Control Eng. Pract.*, vol. 117, Dec. 2021, Art. no. 104931.

[29] A. Loría, "Observers are unnecessary for output-feedback control of Lagrangian systems," *IEEE Trans. Autom. Control*, vol. 61, no. 4, pp. 905–920, Apr. 2016.

[30] I. Sarras, E. Nuño, L. Basañez, and M. Kinnaert, "Position tracking in delayed bilateral teleoperators without velocity measurements," *Int. J. Robust Nonlinear Control*, vol. 26, no. 7, pp. 1437–1455, May 2016.

[31] M. A. Arteaga–Pérez and E. Nuño, "Velocity observer design for the consensus in delayed robot networks," *J. Franklin Inst.*, vol. 355, no. 14, pp. 6810–6829, Sep. 2018.

[32] M. A. Arteaga-Pérez, M. López, E. Nuño, and Ó. Hernández-Ortiz, "On the delayed kinematic correspondence with variable time delays for the control of the bilateral teleoperation of robots," *Int. J. Control*, vol. 94, no. 9, pp. 2353–2368, Sep. 2021.

[33] S. Islam, P. X. Liu, and A. El Saddik, "Observer-based force reflecting robust coordination control for networked bilateral shared telerobotic system," *Int. J. Control*, vol. 92, no. 8, pp. 1858–1869, Aug. 2019.

[34] J. M. Daly and D. W. Wang, "Time-delayed output feedback bilateral teleoperation with force estimation for n-DOF nonlinear manipulators," *IEEE Trans. Control Syst. Technol.*, vol. 22, no. 1, pp. 299–306, Jan. 2014.

[35] L. Chan, F. Naghdy, and D. Stirling, "Position and force tracking for non-linear haptic telemanipulator under varying delays with an improved extended active observer," *Robot. Auto. Syst.*, vol. 75, pp. 145–160, Jan. 2016.

[36] F. Azimifar, K. Hassani, A. H. Saveh, and F. T. Ghomshe, "Performance analysis in delayed nonlinear bilateral teleoperation systems by force estimation algorithm," *Trans. Inst. Meas. Control*, vol. 40, no. 5, pp. 1637–1644, Mar. 2018.

[37] F. Azimifar, S. Ahmadkhosravi Rozi, A. Saleh, and I. Afyouni, "Transparency performance improvement for multi-master multi-slave teleoperation systems with external force estimation," *Trans. Inst. Meas. Control*, vol. 40, no. 13, pp. 3851–3859, Sep. 2018.

[38] A. Barreiro and E. Delgado, "Reset observers alleviating the peaking and the robustness tradeoffs: A case study on force estimation in teleoperation," *ISA Trans.*, vol. 94, pp. 36–46, Nov. 2019.

[39] C. Yang, G. Peng, L. Cheng, J. Na, and Z. Li, "Force sensorless admittance control for teleoperation of uncertain robot manipulator using neural networks," *IEEE Trans. Syst., Man, Cybern., Syst.*, vol. 51, no. 5, pp. 3282–3292, May 2021.

[40] Y. Yuan, Y. Wang, and L. Guo, "Force reflecting control for bilateral teleoperation system under time-varying delays," *IEEE Trans. Ind. Informat.*, vol. 15, no. 2, pp. 1162–1172, Feb. 2019.

[41] S. A. M. Dehghan, H. R. Koofigar, H. Sadeghian, and M. Ekramian, "Observer-based adaptive force-position control for nonlinear bilateral teleoperation with time delay," *Control Eng. Pract.*, vol. 107, Feb. 2021, Art. no. 104679.

[42] A. Mehrjouyan, M. B. Menhaj, and M. A. Khosravi, "Robust observer-based adaptive synchronization control of uncertain nonlinear bilateral teleoperation systems under time-varying delay," *Measurement*, vol. 182, Sep. 2021, Art. no. 109542.

[43] C. P. Vo, X. D. To, and K. K. Ahn, "A novel force sensorless reflecting control for bilateral haptic teleoperation system," *IEEE Access*, vol. 8, pp. 96515–96527, 2020.

[44] B. Siciliano, L. Sciavicco, L. Villani, and G. Oriolo, *Robotics: Modelling, Planning and Control*. Berlin, Germany: Springer, 2010.

[45] M. A. Arteaga, A. Gutiérrez-Giles, and J. Pliego-Jiménez, *Local Stability and Ultimate Boundedness in the Control of Robot Manipulators*. Berlin, Germany: Springer, 2022, doi: 10.1007/978-3-030-85980-0_3.

[46] Y. Yokokohji and T. Yoshikawa, "Bilateral control of master-slave manipulators for ideal kinesthetic coupling-formulation and experiment," *IEEE Trans. Robot. Autom.*, vol. 10, no. 5, pp. 605–620, Oct. 1994.

[47] A. Gutiérrez-Giles and M. A. Arteaga-Pérez, "GPI based velocity/force observer design for robot manipulators," *ISA Trans.*, vol. 53, no. 4, pp. 929–938, Jul. 2014.

[48] R. Kelly, V. Santibánez-Dávila, and J. A. Loria-Perez, *Control of Robot Manipulators in Joint Space*. Berlin, Germany: Springer, 2006.

[49] E. Fridman, *Introduction to Time-Delay Systems: Analysis and Control*. Berlin, Germany: Springer, 2014.

[50] M. A. Arteaga-Pérez and A. Gutiérrez-Giles, "On the GPI approach with unknown inertia matrix in robot manipulators," *Int. J. Control*, vol. 87, no. 4, pp. 844–860, Apr. 2014.

[51] H. Sira-Ramirez, A. Luviano-Juarez, M. Ramirez-Neria, and E. W. Zurita-Bustamante, *Active Disturbance Rejection Control of Dynamic Systems: A Flatness Based Approach*. Oxford, U.K.: Butterworth-Heinemann, 2018.

[52] H. K. Khalil, *Nonlinear Systems*. Upper Saddle River, NJ, USA: Prentice-Hall, 2002.

[53] M. Vidyasagar, *Nonlinear Systems Analysis*. Philadelphia, PA, USA: SIAM, 2002.

[54] M. D. Ferdinando, P. Pepe, and A. Borri, "On practical stability preservation under fast sampling and accurate quantization of feedbacks for nonlinear time-delay systems," *IEEE Trans. Autom. Control*, vol. 66, no. 1, pp. 314–321, Jan. 2021.

[55] Ó. Hernández-Ortiz and M. A. Arteaga-Pérez, "A simple approach for the force control of bilateral teleoperated manipulators with variable time delays," *Control Eng. Pract.*, vol. 102, Sep. 2020, Art. no. 104564.